NATIONAL ADVISORY COMMITTEE FOR AERONAUTICS

TECHNICAL NOTE

No. 1111

INVESTIGATION OF THE EFFECT OF A TIP MODIFICATION AND THERMAL DE-ICING AIR FLOW ON PROPELLER PERFORMANCE

By Blake W. Corson, Jr. and Julian D. Maynard

Langley Memorial Aeronautical Laboratory
Langley Field, Va.

Washington
July 1946

NATIONAL ADVISORY COMMITTEE FOR AERONAUTICS

TECHNICAL NOTE NO. 1111

INVESTIGATION OF THE EFFECT OF A TIP MODIFICATION AND THERMAL DE-ICING AIR FLOW ON PROPELLER PERFORMANCE

By Blake W. Corson, Jr. and Julian D. Maynard

SUMMARY

Aerodynamic tests of a 12.208-foot-diameter two-blade hollow steel propeller before and after alteration for thermal de-icing have been made in the Langley 16-foot high-speed tunnel to determine the effect of the alterations on propeller efficiency. The propeller, which had Clark Y blade sections, was tested on a 2000-horsepower dynamometer at blade angles ranging from about 25° to 60° at the 42-inch radius and at airspeeds varying from 100 to 425 miles per hour.

The loss of propeller envelope efficiency due to the tip alteration without internal air flow amounted to about $1\frac{1}{2}$ percent at the lower values of advance ratio and decreased to about $\frac{1}{2}$ percent at an advance ratio of 2.8. The over-all loss of propeller efficiency due to the tip alteration with internal air flow amounted to about 3 percent at the lower values of advance ratio and decreased to about $\frac{1}{2}$ percent at an advance ratio of 2.8. An increase in helical tip Mach number from 0.75 to 0.88 had little or no effect on the loss of propeller efficiency caused by the internal air flow. The coefficient of mass flow of de-icing air increased with propeller advance ratio and decrased with increase in rotational speed for the particular thermal de-icing propeller used in the tests.

INTRODUCTION

The hazards due to the formation of ice on propellers are becoming increasingly serious for large multiengine airplanes for which cruising efficiency and propeller unbalance on long flights are important. The trend of propeller design for airplanes of this type is more and more toward propellers of large diameter and low rotational speed. De-icing methods used with moderate success in the past on relatively small propellers have been found inadequate for the large-diameter propellers. The alcohol slinger ring used for de-icing in the past presents the difficulty of obtaining adequate blade coverage for the larger, slower-turning propellers. The use of anti-icing pastes and lacquers on propeller blades is a simple solution to the problem, but the effective service life of such compounds is known to be short. A positive method of de-icing the propeller at all times of operation would be more desirable. There has been appreciable development during the past few years of electrical de-icing propellers which have hub generators supplying current to conductive rubber-heating elements cemented to the blades. The energy per unit weight of the hub generator used in these propellers is proportional to the rotational speed, so that a heavier generator would be required for propellers of slower rotation and large diameter. Should slip rings be used to supply electrical heating to the larger blades the energy required might be beyond the capacity of the normal aircraft electrical system, and an auxiliary generator engine would be necessary.

A logical method of propeller de-icing seems to be one which makes use of the heat in the engine exhaust gases. This heat might be used by passing the engine exhaust through heat exchangers from which hot air could flow to a hollow hub and thence through openings in the blade shanks to the tips of hollow steel blades. The principal alteration of the propeller necessary to permit this flow of heated air is the provision of openings, or nozzles, at the tips of the propeller blades to allow the heated air to pass into the slipstream. The purpose of the present tests is to determine the effects of such tip modifications on propeller performance and also the effects of the internal air flow on propeller performance. No attempt is made to simulate the complete de-icing system. The tests were made in the Langley 16-foot high-speed tunnel.

A theoretical analysis of the losses associated with a thermal de-icing propeller of the type tested was considered too voluminous to be included herein. The theoretical treatment is presented in reference 1, which correlates the calculated with the experimental results presented herein.

APPARATUS

Propeller dynamometer.- A 2000-horsepower propeller dynamometer with a rated speed of 2100 rpm was used in testing the propellers. Figures 1 and 2 are photographs of the dynamometer with the test propeller in its normal unaltered condition (without tip openings) in the test section of the wind tunnel. The dynamometer is powered by two 1000-horsepower electric motors arranged in tandem and coupled for the present tests so that the power of both motors could be expended through a single propeller. The motors are supported in a housing in such a way that their casings are free to rotate and also free to move axially with their shafts. The axial and rotational movement is restrained by pneumatic pressure capsules, thrust and torque being proportional to the pressure required to restrain the motion. A more detailed description of the dynamometer is given in reference 2. The nose spinner and two propeller spinners described in reference 2 were not used in the present tests; the propeller hub was left exposed to the air stream about 1 inch forward of a nose cowling rigidly attached to the dynamometer fairing. The outline of this nose cowling may be seen in figure 3, which is a sketch showing principal dimensions of the dynamometer in the test section of the wind tunnel.

Propeller blades.- The propeller used in the tests consisted of two Curtiss hollow steel blades with Clark Y sections, design number 714-1C2-12, fitted to a four-way hub. This combination gave a propeller 12.208 feet in diameter. The two unused hub openings were filled with solid dural blanks. Blade-form curves are shown in figure 4 with the location of the tip nozzle indicated on the developed plan form. Photographs of these tip openings, which are in the cambered face of the blades near the trailing edge, are shown in figures 5, 6, and 7. Figure 8 is a sketch showing the way in which the hollow steel blade tips were cut to form the nozzles, which were enlarged by a small bulge in the cambered surface of each blade. Each tip nozzle had a cross-sectional area of 0.65

square inch, making the total nozzle area for the two blades 0.00903 square foot. The tip nozzle was a manufacturer's design and was believed to be of sufficient size to permit adequate de-icing air flow through each blade; however, the quantity of de-icing air flow required has not been definitely established. Recent indications are that the tip nozzle in the blades tested was larger than necessary.

Metering orifice.- Inasmuch as the purpose of the present tests was only to determine the effects of the tip modifications and of the internal air flow on propeller performance, no attempt was made either to heat the "de-icing air" or to control the rate of flow. This de-icing air was admitted through a bellmouthed orifice in the front of the propeller hub and then passed through a Y-duct into the blade shanks. From the shanks the air flowed through the hollow blades from hub to tip and thence through the tip openings into the propeller slipstream. Figure 9 is a photograph of the propeller hub with the bellmouthed orifice attached. The orifice is 1.25 inches in diameter, and a static-pressure tube located in the orifice has a diameter of 0.25 inch. The resulting orifice area is 0.00818 square foot. The static-pressure tube located in the orifice was necessary to determine the internal mass flow.

Pressure seal.- The pressure lead from the static tube extended through the hollow shaft of the dynamometer and rotated with the shaft. The pressure was transmitted from the rotating shaft by means of a small steel tube (0.050-inch diameter) turning in a soft rubber seal slightly lubricated with glycerin. This seal operated very satisfactorily during the entire series of tests. Figure 10 is a sketch of a section through the bellmouthed orifice, propeller hub, hollow steel blade, dynamometer shaft, and pressure seal showing the complete path of the internal flow and the means of measuring the internal mass flow. Static pressure in the orifice was measured by a micromanometer referenced to atmospheric pressure as indicated in figure 10.

TESTS

The propeller was tested in three conditions: first, as a normal propeller without tip openings; second, as a propeller with tip openings but without de-icing air flow; and finally, as a propeller with de-icing air flow. In each condition the propeller was operated at a series of fixed blade angles ranging from approximately 25° to 60° at the 42-inch radius. Blade angles at the three-quarter (54-inch) radius are less by 6.1°. Each test was made at a constant rotational speed, and a range of advance ratio was covered for each blade angle by changing the tunnel airspeed which was varied from about 100 miles per hour to 425 miles per hour.

The propeller used for the tests is a Curtiss propeller designed for application to a large bomber. This propeller has three blades, is 19 feet in diameter, and has a rotational speed of 784 rpm at take-off and military power. At normal power, the rotational speed is 740 rpm. By operating the test propeller at 1240 rpm, tip speeds were obtained which equaled those obtained with the 19-foot-diameter propeller turning at 784 rpm. At the higher blade angles the dynamometer would not deliver sufficient torque to cover the complete range of advance ratio at 1240 rpm, and therefore the test rotational speed was reduced to a lower value to provide data at the lower values of advance ratio. A rotational speed of 1000 rpm was used for tests at blade angles of 50° and 55°; a rotational speed of 800 rpm was used for tests at a blade angle of 60°; and tests at the remaining blade angles of 25°, 30°, 35°, 40°, and 45° were made at the rotational speed of 1240 rpm. The propeller was also tested at 1450 rpm for blade angles of 30° and 35°. At this rotational speed the propeller tip Mach number was approximately the same as that for the large bomber propeller for the high-speed condition at 35,000 feet altitude. These tests at 1450 rpm were made to determine the effect of the internal air flow on propeller efficiency under conditions conducive to compressibility loss.

The mass flow of de-icing air was measured during all tests of the propeller with de-icing air flow. At each blade angle, a few measurements of de-icing air flow were made at several rotational speeds but at a constant value of advance ratio. For these tests, values of advance ratio were chosen so that a blade section at the tip would operate at approximately zero angle of attack to minimize the effect of aerodynamic suction at the tip opening. Also, the mass flow of de-icing air was measured over a range of tunnel airspeeds with the dynamometer motors not operating and with the propeller blades set at 88.7° at the 42-inch radius. In this condition the propeller was free to windmill, but the rotational speed was very small so that the advance ratio was nearly infinite.

REDUCTION OF DATA

Symbols.- The test results corrected for tunnel-wall interference are presented in the form of the usual thrust and power coefficients and propeller efficiency. The mass flow of de-icing air determined from the test data is also presented in coefficient form. The symbols and definitions used are as follows:

A_o area of metering orifice, square feet

A_N total tip-nozzle area, square feet

V airspeed, free stream, feet per second

V_d wind-tunnel datum velocity, feet per second

V_N velocity of air leaving nozzle, feet per second

V_o velocity of air in metering orifice where area is A_o, feet per second

ρ mass density of air, free stream, slugs per cubic foot

ρ_N mass density of internal flow at the nozzle, slugs per cubic foot

ρ_o mass density of air in metering orifice where V_o exists, slugs per cubic foot

p_o static pressure in metering orifice where V_o exists, pounds per square foot

p_a atmospheric pressure, pounds per square foot

Δp pressure change in metering orifice ($\Delta p = p_a - p_o$), pounds per square foot

Δp_f	pressure loss across the internal flow system, pounds per square foot
q_N	dynamic pressure at the nozzle, pounds per square foot $\left(\frac{1}{2}\rho_N V_N^2\right)$
t_a	atmospheric temperature, $^{\circ}F$ absolute
g	acceleration due to gravity (32.2 ft/sec^2)
R	universal gas constant (53.34 ft-lb/lb $^{\circ}F$ for air)
γ	ratio of specific heats (1.40 for air)
M	Mach number
n	propeller rotational speed, rps
D	propeller diameter, feet
J	propeller advance ratio (V/nD)
J_d	nominal propeller advance ratio based on tunnel datum velocity
μ	Glauert's velocity correction for wind-tunnel wall interference ($V = \mu V_d$; $J = \mu J_d$)
x	fraction of propeller tip radius
β	blade angle, degrees
h	blade section maximum thickness, feet
b	blade chord, feet
P	power absorbed by the propeller, foot-pounds per second
C_P	power coefficient ($P/\rho n^3 D^5$)
T	propeller thrust, pounds
C_T	thrust coefficient ($T/\rho n^2 D^4$)
η	propeller efficiency $\left(\frac{C_T}{C_P}J\right)$

m mass flow rate of de-icing air, slugs per second

m_c coefficient of mass flow of de-icing air ($m/\rho A_N nD$)

Correction for wind-tunnel wall interference.- When a propeller operates in an air stream constrained by wind-tunnel walls, the velocity indicated by the wind-tunnel calibrated orifices is greater than the velocity in free air at which the propeller would produce the same thrust and torque at the same rotational speed as used in the wind tunnel. A correction must be applied to the tunnel datum velocity to obtain the corresponding free-stream airspeed. Glauert, in reference 3, has made an analysis in which he shows this correction to be a function of the ratio of propeller thrust to dynamic pressure, or ratio of thrust coefficient to nominal advance ratio. The equivalent free airspeed has been determined experimentally and found to agree well with values calculated from Glauert's equation; hence only the theoretical correction has been used for the data obtained in these tests. A plot of Glauert's velocity correction for a propeller 12.208 feet in diameter operating in a 16-foot-diameter closed jet tunnel is shown in figure 11. Also in figure 11 is a curve showing values of advance ratio for the normal propeller at the peak efficiency condition plotted against the ratio C_T/J_d^2. The curves show that for the peak efficiency condition the correction for wind-tunnel wall interference amounted to less than 2 percent at all values of advance ratio above 0.86 and to less than 1 percent at all values above 1.6. The maximum correction for any condition of operation was approximately 6 percent (lowest value of advance ratio for the lowest blade angle).

Definition of propeller thrust.- Propeller thrust, as used herein, is defined as the increase in shaft tension caused by the rotation of the propeller and hub in the air stream.

Definition and determination of the coefficient of mass flow.- In order to be consistent with other propeller coefficients, the coefficient of mass flow of de-icing air is defined as follows:

$$m_c = \frac{m}{\rho A_N n D} \qquad (1)$$

by continuity the mass flow m at the tip nozzle is

$$m = A_o \rho_o V_o \qquad (2)$$

where A_o, ρ_o, and V_o are the area, density, and velocity at the metering orifice. If reversible adiabatic flow is assumed, the density at the metering orifice may be expressed in terms of measured values of the pressure differential Δp and the total pressure and temperature. In the wind tunnel the total pressure in the throat is equal to the static pressure in the quiescent chamber or essentially equal to atmospheric pressure (barometric pressure). Also, the stagnation temperature in the throat is equal to the temperature in the quiescent chamber. The density at the metering orifice, therefore, may be expressed as follows:

$$\rho_m = \frac{p_a}{gRt_a}\left(1 - \frac{\Delta p}{p_a}\right)^{\frac{1}{\gamma}} \qquad (3)$$

The velocity at the metering orifice may be expressed in the same terms as those used in equation (3) by use of Bernoulli's equation for compressible adiabatic flow. Solving for velocity gives the equation

$$V_o = \sqrt{\frac{2\gamma}{\gamma - 1} gR}\ \sqrt{t_a}\sqrt{1 - \left(1 - \frac{\Delta p}{p_a}\right)^{\frac{\gamma-1}{\gamma}}} \qquad (4)$$

Substituting the expressions for density and velocity (equations (3) and (4)) into equation (2) gives

$$m = A_o \frac{p_a}{gRt_a}\left(1 - \frac{\Delta p}{p_a}\right)^{\frac{1}{\gamma}}\sqrt{\left(\frac{2\gamma}{\gamma - 1}\right)gR}\ \sqrt{t_a}\ \sqrt{1 - \left(1 - \frac{\Delta p}{p_a}\right)^{\frac{\gamma-1}{\gamma}}} \qquad (5)$$

Simplifying and expanding this equation results in the following expression:

$$m = A_o \sqrt{\frac{2\gamma}{(\gamma - 1)gR}} \frac{p_a}{\sqrt{t_a}} \sqrt{0.285 \frac{\Delta p}{p_a} - 0.305 \left(\frac{\Delta p}{p_a}\right)^2}$$

RESULTS AND DISCUSSION

Faired curves are presented of thrust coefficient, power coefficient, propeller efficiency, and the coefficient of mass flow of de-icing air plotted against advance ratio. In the figures giving thrust coefficient, power coefficient, and coefficient of mass flow of de-icing air, the test points are shown. Data for the normal propeller are shown in figures 12 to 14; data for the altered propeller operating without de-icing air flow are shown in figures 15 to 20; and data for the propeller operating with de-icing air flow are presented in figures 21 to 30. Figure 31 is included to show the variation of air-stream Mach number and helical tip Mach number with advance ratio for the different rotational speeds used in the tests. The envelope curves of propeller efficiency for the three conditions of the propeller are compared in figure 32.

Accuracy.- The results obtained from several repeat tests of the propeller in the three conditions of operation agreed with the presented results within 1 percent. For purposes of comparison, therefore, the data are presented as accurate to within 1 percent and the faired envelopes as accurate to within much closer limits.

Effect of tip alteration.- A comparison of figure 12 with figure 15 shows that cutting the blade tips to provide openings reduced the propeller thrust. The tip alteration had only a small effect on power absorption, as shown by a comparison of the power coefficient curves in figure 13 with those in figure 16. Figure 32 shows that the loss of thrust caused a loss of propeller efficiency amounting to about $1\frac{1}{2}$ percent at the lower values of advance ratio, decreasing to about $\frac{1}{2}$ percent at an advance ratio of 2.8.

Effect of internal air flow.- The flow of de-icing air had only a small effect on the propeller thrust and power coefficients. This effect is shown by comparing the thrust- and power-coefficient curves in figures 15 and 16 with those in figures 21 and 22. A comparison of the envelope curves of propeller efficiency in figure 32 shows that the additional loss of efficiency caused by the internal air flow amounted to about $\frac{1}{2}$ percent or less over most of the range of advance ratio. At some of the lower values of advance ratio, however, this loss was as much as $1\frac{1}{2}$ percent.

Effect of compressibility.- A difference in the slope of both the thrust- and power-coefficient curves at the different test rotational speeds may be seen in figures 12, 13, 15, 16, 21, and 23. This difference may be due to a change in the characteristics of the blade sections with change in Reynolds number or, more likely, with change in Mach number; however, the values of peak efficiency were little affected.

Although the helical tip Mach number of the propeller was from 0.84 to 0.88 in the tests made at 1450 rpm, the loss in propeller efficiency caused by the tip alteration was about the same for these tests as for the tests made at 1240 rpm (helical tip Mach number about 0.75). Figures 18, 19, and 20 show the thrust-coefficient, power-coefficient, and propeller-efficiency curves for the tests made at 1450 rpm without de-icing air flow. The data for the condition with de-icing air flow at 1450 rpm are shown in figures 24, 25, and 26. The values of propeller efficiency shown in figure 26 indicate that the loss in efficiency caused by the internal air flow was little or no greater at the high tip speeds than at the lower tip speeds.

Coefficient of mass flow of de-icing air.- Figures 27 and 28 show the variation of the coefficient of mass flow of de-icing air with advance ratio for the different rotational speeds and blade angles used in the tests. The relation between coefficient of mass flow and advance ratio may be expressed by the following equation which is derived in reference 1:

$$m_c = \left(\frac{\rho_N}{\rho}\right)\sqrt{\frac{(\pi x)^2 + J^2}{\frac{\Delta p_f}{q_N} + 1}} \qquad \text{(equation (27) of reference 1)}$$

where $\frac{\Delta p_f}{q_N}$ is the internal pressure loss expressed as a ratio to the dynamic pressure of the nozzle jet. The internal loss is the combined resistance offered to the internal flow by the skin friction of the interior surface of the blades; by turbulence introduced in the flow by abrupt turns, sharp corners, and poor nozzle shape; by inefficient diffusion; and by changes in flow pattern with rotational speed typical of centrifugal blowers. Curves of the form defined by the foregoing equation were fitted to the test data presented in figures 27 and 28, and values of the constants were established as follows (from fig. 8 of reference 1):

Rotational speed (rpm)	$\frac{\Delta p_f}{q_N}$	$\frac{\rho_N}{\rho}$
1450	1.465	0.925
1240	1.270	.942
1000	1.092	.955
800	.998	.963
0	.930	.986

The fitted curves are presented as dashed lines in figures 27 and 28. The close agreement between the trends of the data and the fitted curves indicates that the form of the equation is satisfactory.

The effect of rotational speed on the mass-flow coefficient is shown in figure 29, which presents the data for the tests made at several rotational speeds but at constant values of advance ratio. An increase in rotational speed is accompanied by a decrease in the coefficient of mass flow, due perhaps to an increase in the internal pressure loss. This effect may possibly be explained by changes of the internal flow pattern with changes in rotational speed and blade angle. Figure 30 shows the mass-flow data obtained in the test made with the propeller feathered and the rotational speed almost zero. When the rotational speed is zero, the advance ratio becomes infinite; and the equation for the mass-flow coefficient from reference 1 may be revised as follows:

$$\frac{m_c}{J} = \frac{\frac{\rho_N}{\rho}}{\sqrt{\frac{\Delta p_f}{q_N} + 1}}$$

Also,

$$\frac{m_c}{J} = \frac{m}{\rho A_N V}$$

The curve in figure 30 shows that the value of $\frac{m_c}{J}$ for the thermal de-icing propeller tested was constant at 0.705 over most of the speed range, and it may be concluded that $\frac{\Delta p_f}{q_N}$ and $\frac{\rho_N}{\rho}$ did not change within the range of these tests.

CONCLUSIONS

High-speed wind-tunnel tests of a full-scale two-blade propeller with a tip modification to permit air flow through the hollow steel blades for thermal de-icing led to the following conclusions:

1. The loss of propeller envelope efficiency due to the tip alteration without flow amounted to about $1\frac{1}{2}$ percent at the lower values of advance ratio and decreased to about $\frac{1}{2}$ percent at an advance ratio of 2.8.

2. The over-all loss of propeller envelope efficiency due to the tip alteration with de-icing air flow amounted to about 3 percent at the lower values of advance ratio and decreased to about $\frac{1}{2}$ percent at an advance ratio of 2.8.

3. An increase in helical tip Mach number from 0.75 to 0.88 had little or no effect on the loss of propeller efficiency caused by the internal air flow.

4. The coefficient of mass flow of de-icing air increased with increase in propeller advance ratio and decreased with increase in rotational speed for the particular thermal de-icing propeller used in the tests.

Langley Memorial Aeronautical Laboratory
National Advisory Committee for Aeronautics
Langley Field, Va., May 7, 1946

REFERENCES

1. Corson, Blake W., Jr., and Maynard, Julian D.: Analysis of Propeller Efficiency Losses Associated with Heated-Air Thermal De-Icing. NACA TN No. 1112, 1946.

2. Corson, Blake W., Jr., and Maynard, Julian D.: The Effect of Simulated Icing on Propeller Performance. NACA TN No. 1084, 1946.

3. Glauert, H.: The Elements of Aerofoil and Airscrew Theory. American ed., The MacMillan Co., 1943, pp. 222-226.

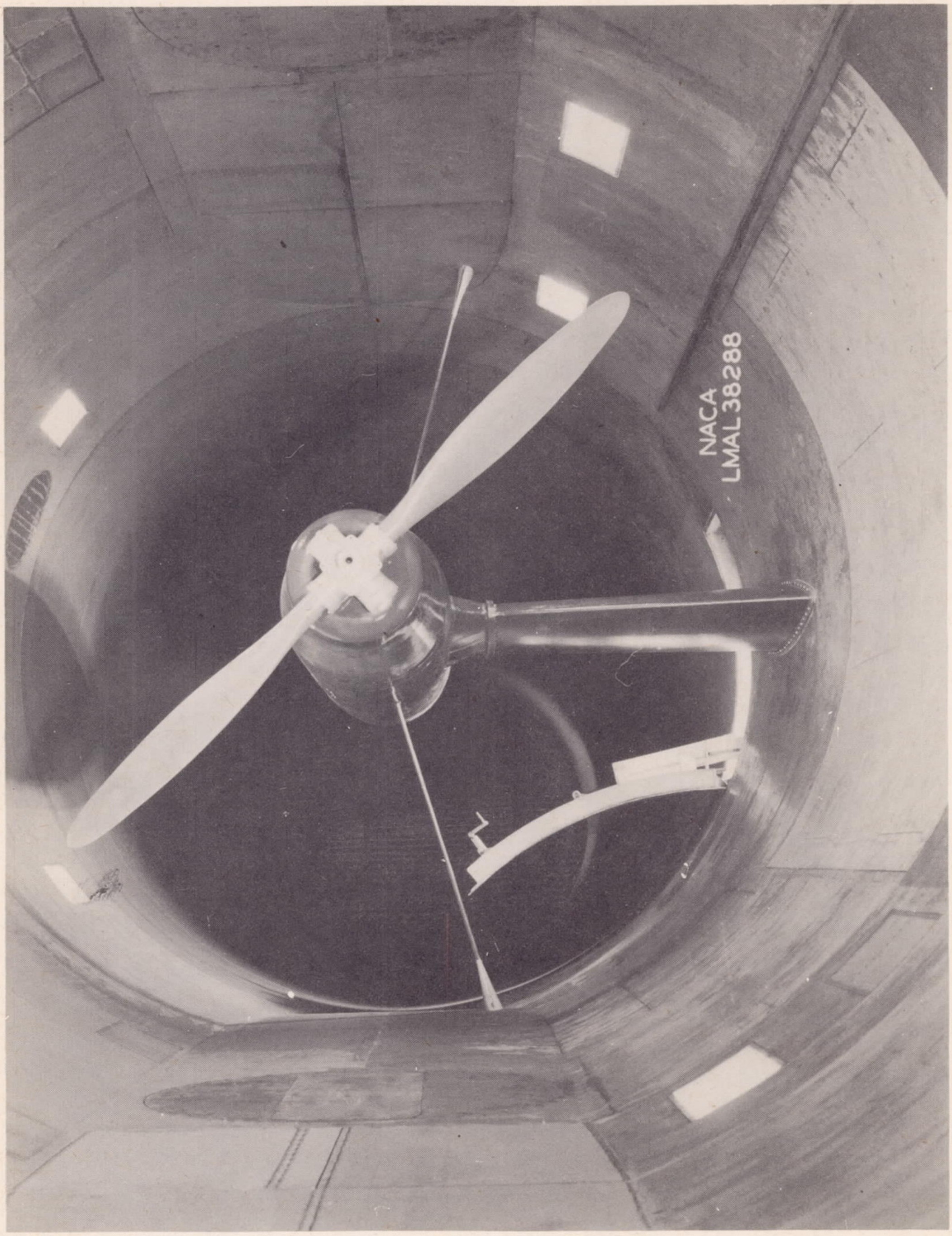

Figure 1.- Propeller dynamometer mounted in test section. Normal propeller.

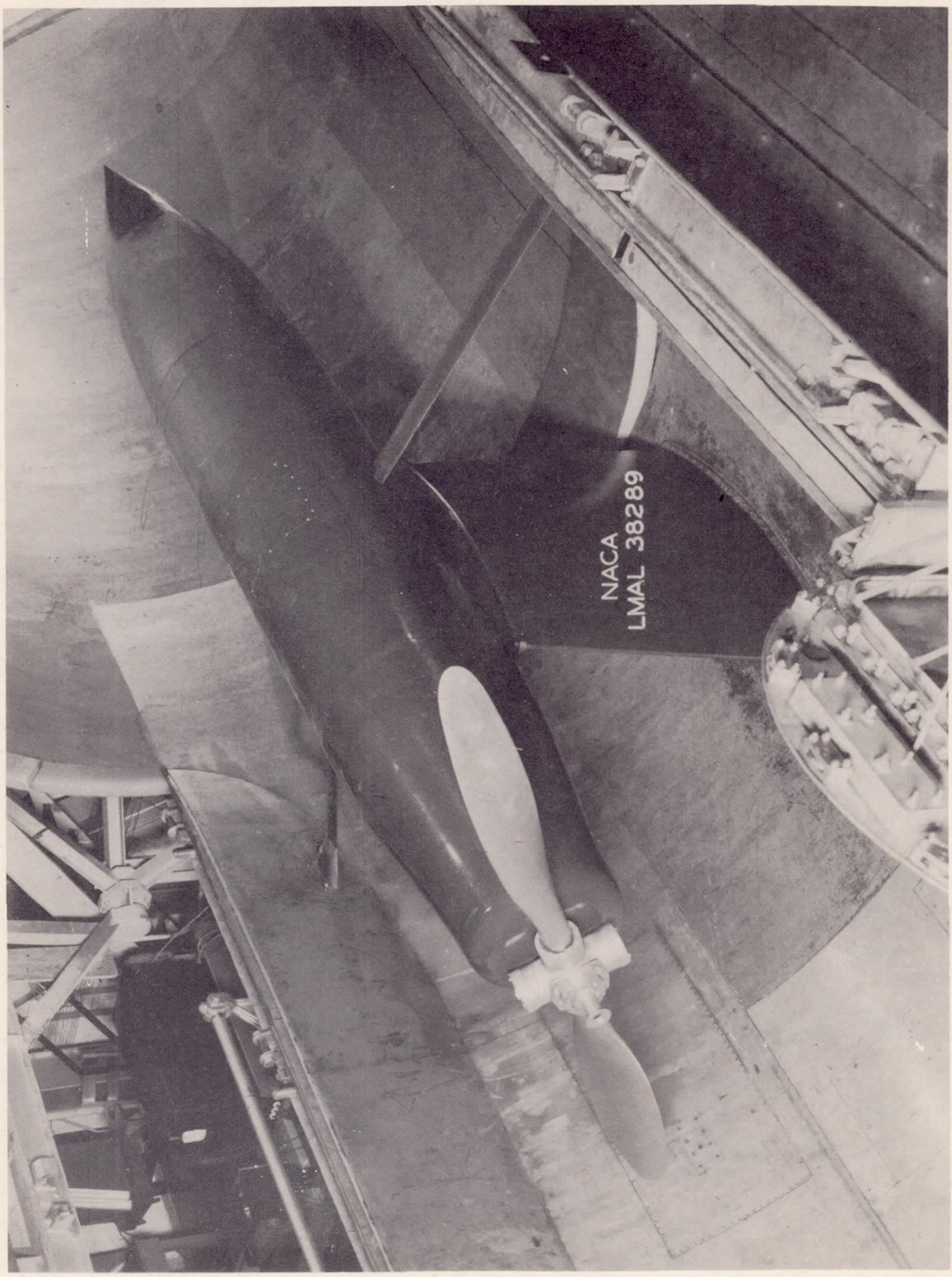

Figure 2.- Propeller dynamometer mounted in test section. Normal propeller, tunnel open.

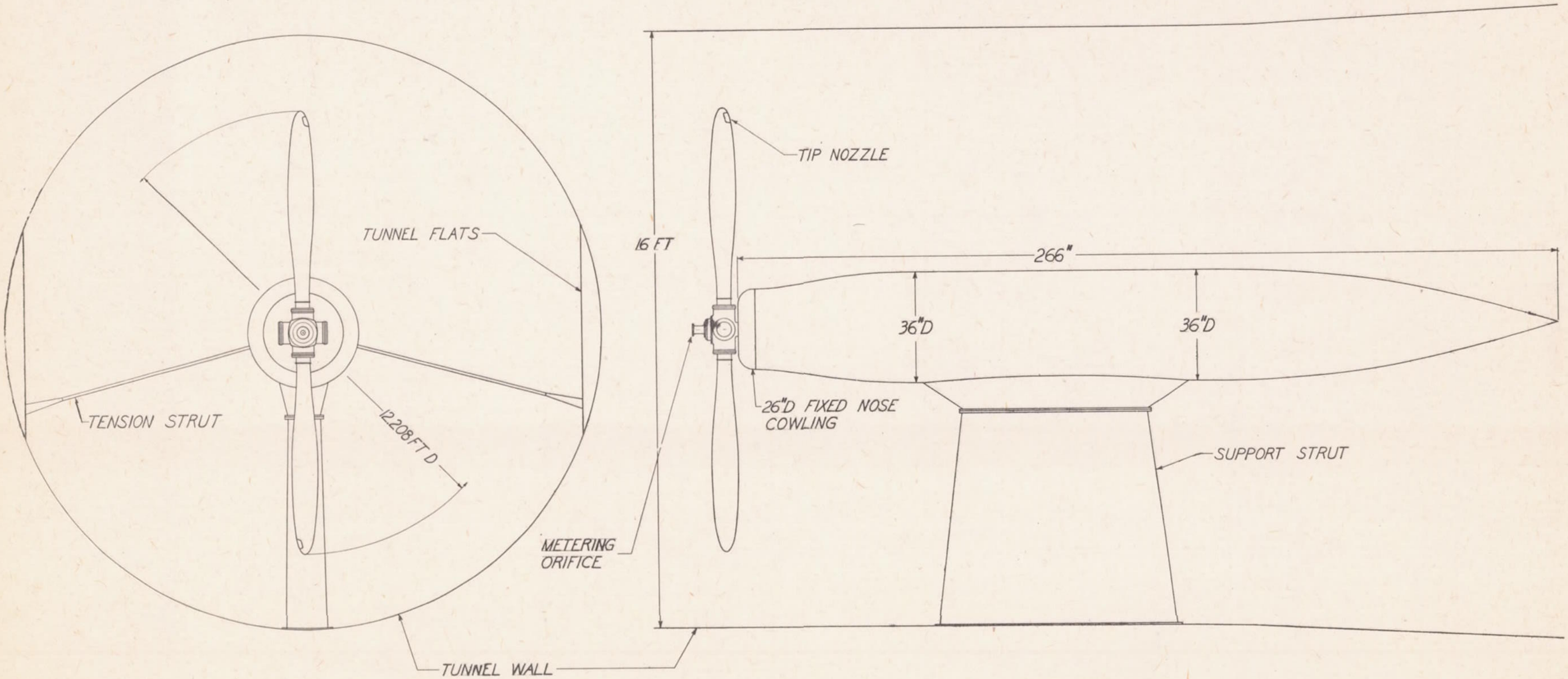

NATIONAL ADVISORY COMMITTEE FOR AERONAUTICS.

FIGURE 3.— CONFIGURATION OF DYNAMOMETER FOR TESTS OF THERMAL DE-ICING PROPELLER.

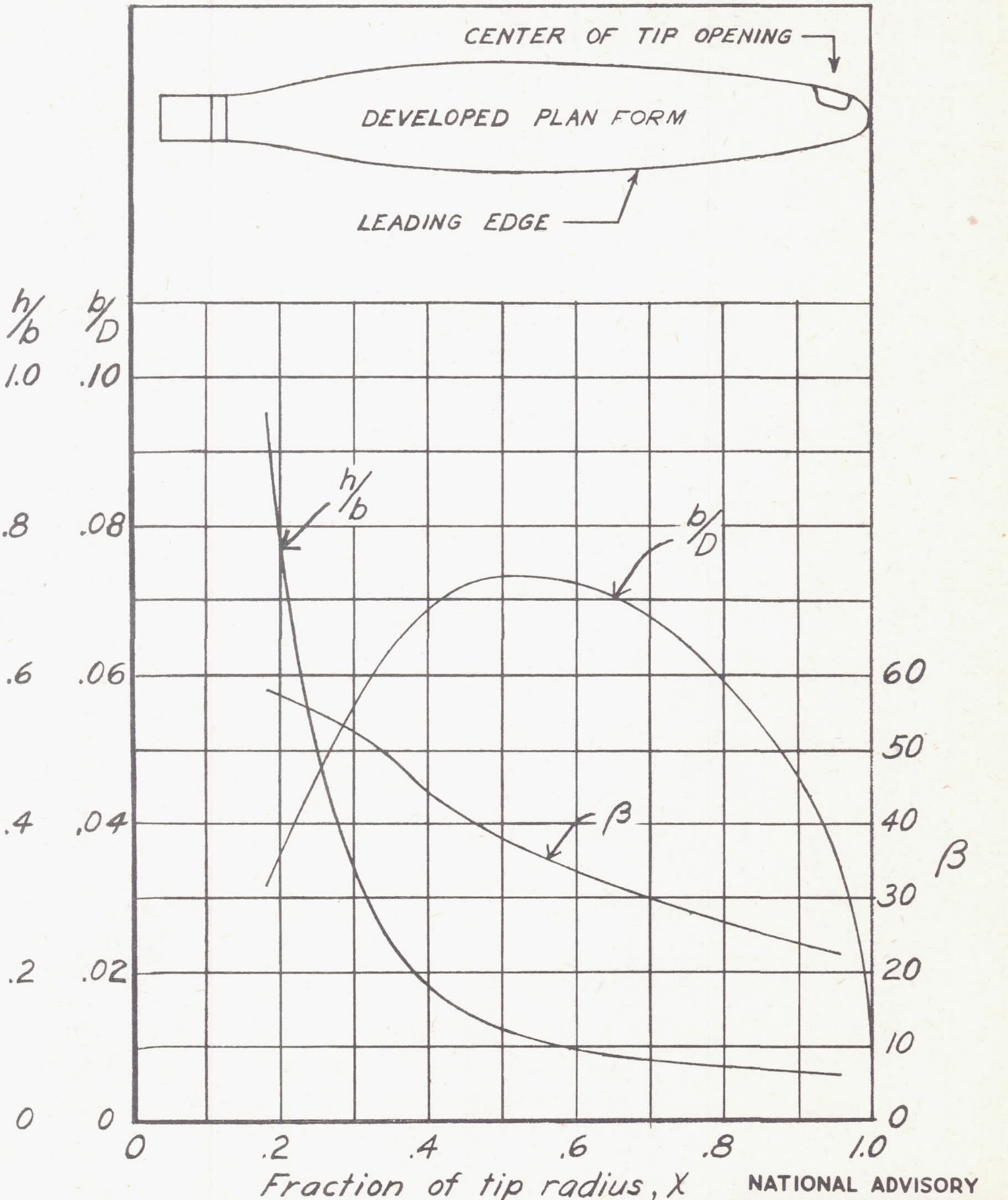

Figure 4.- Blade form curves for Curtiss 714-1C2-12 propeller.

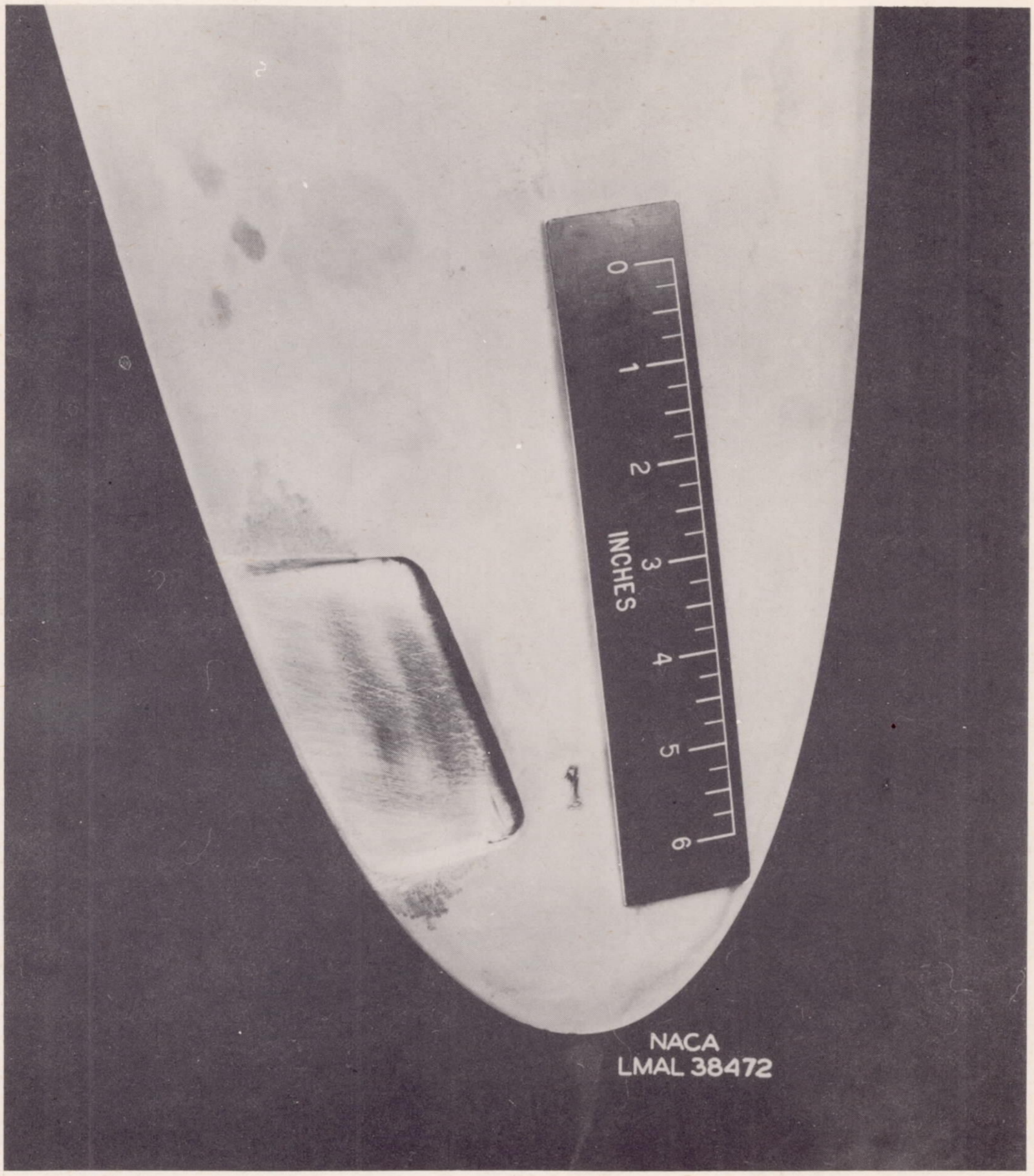

Figure 5.- Tip opening in blade 1.

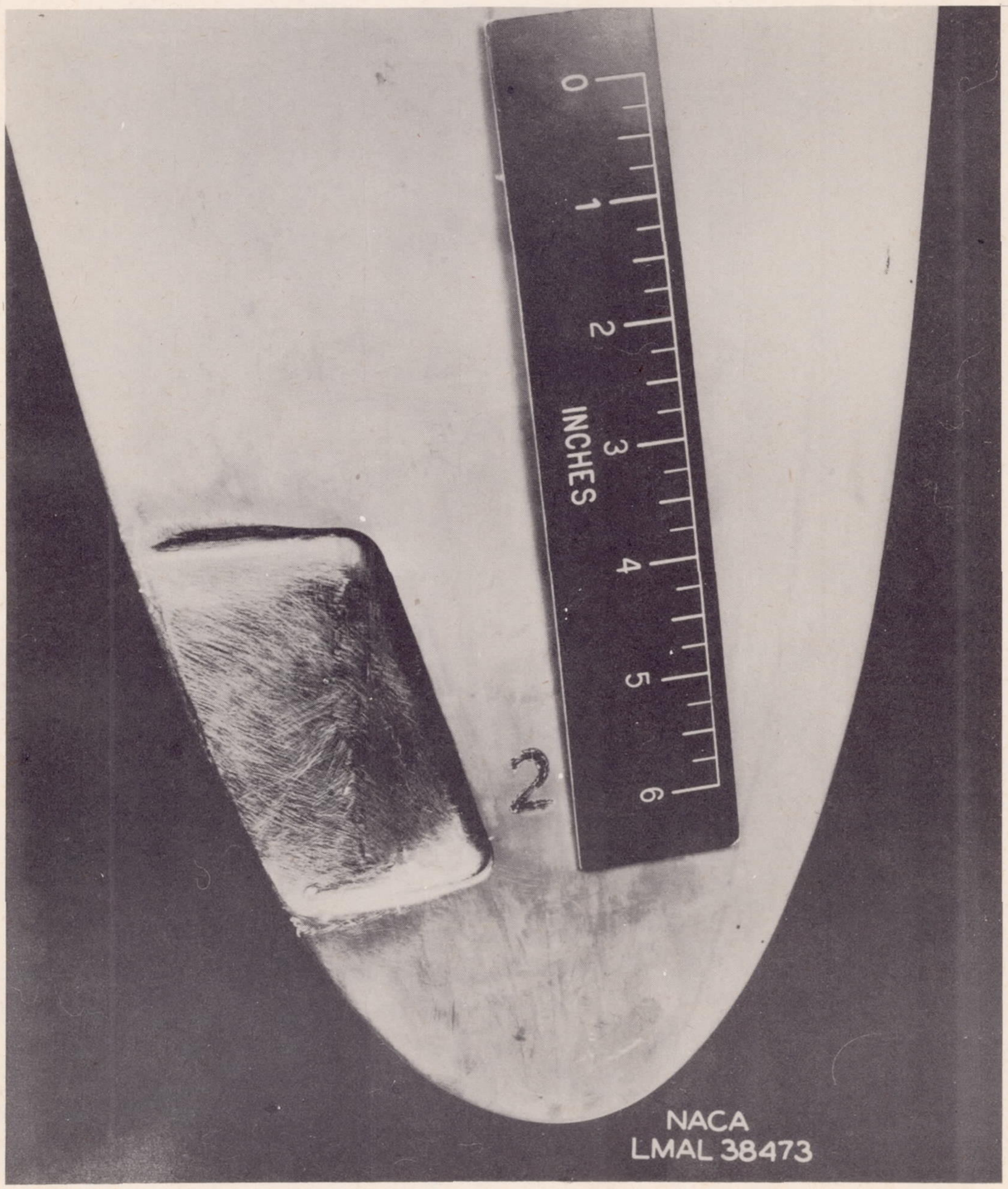

Figure 6.- Tip opening in blade 2.

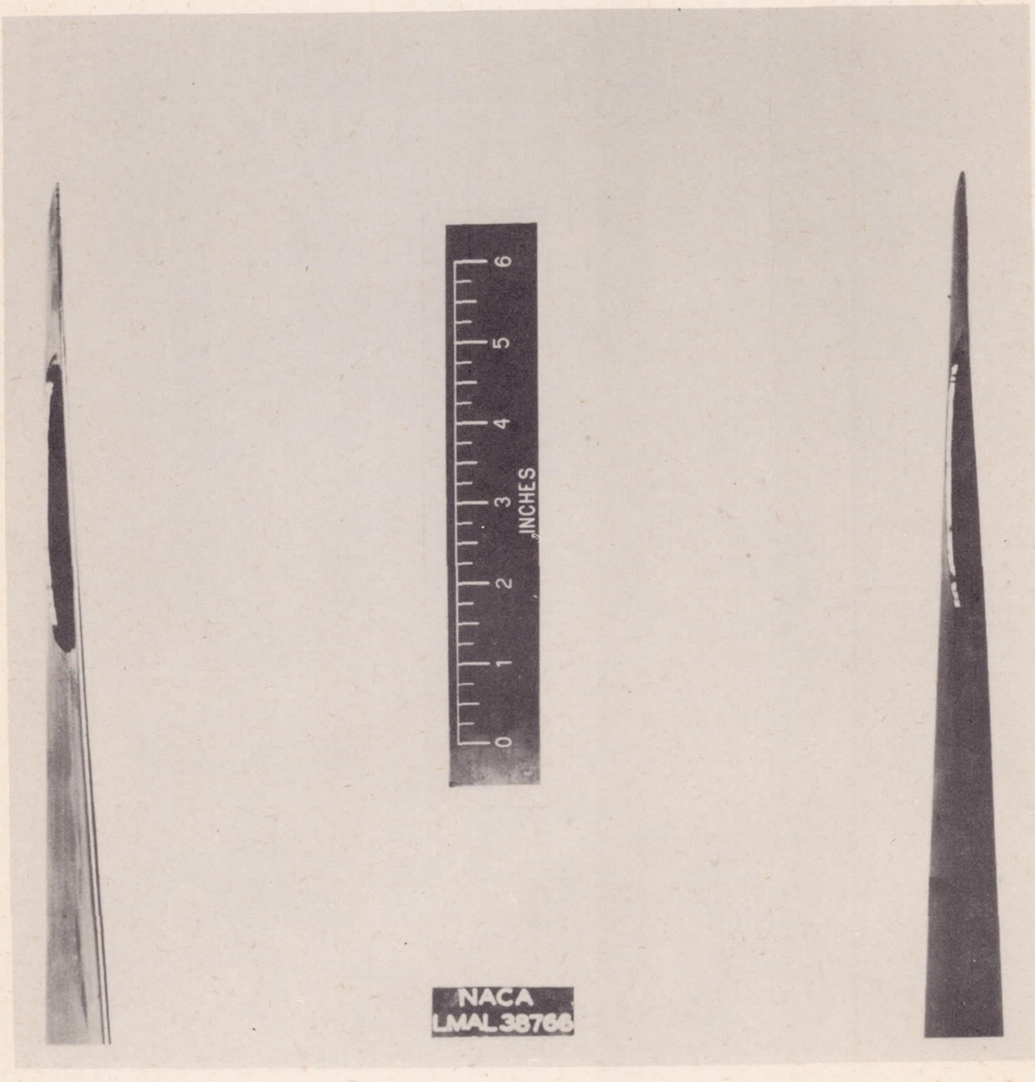

Blade 1

Blade 2

Figure 7.- Trailing-edge view of tip openings in blades 1 and 2.

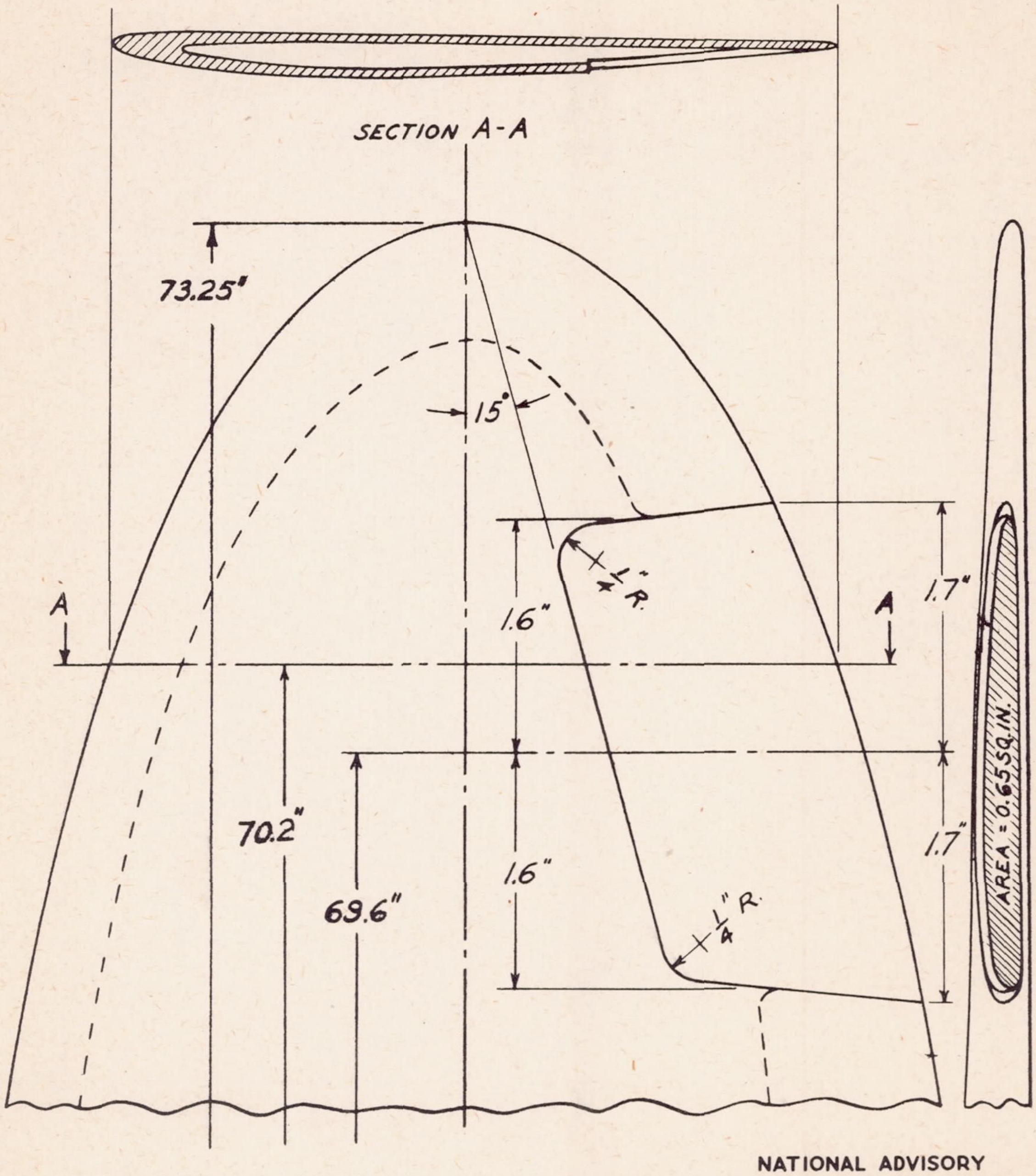

NATIONAL ADVISORY
COMMITTEE FOR AERONAUTICS

FIGURE 8.- APPROXIMATE DIMENSIONS OF THE TIP OPENING IN THE CURTISS 714-1C2-12 PROPELLER.

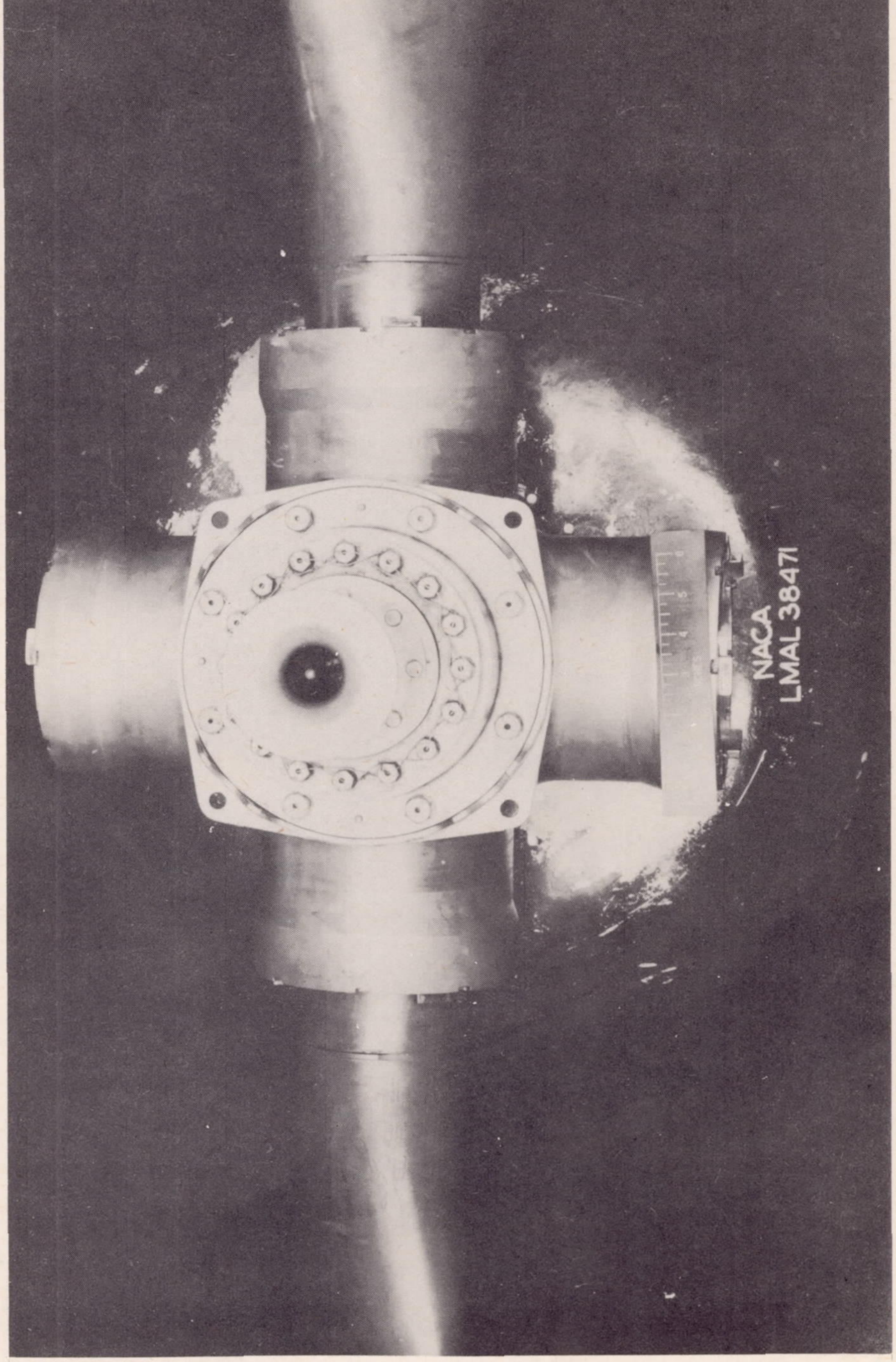

Figure 9.- Propeller hub and metering device.

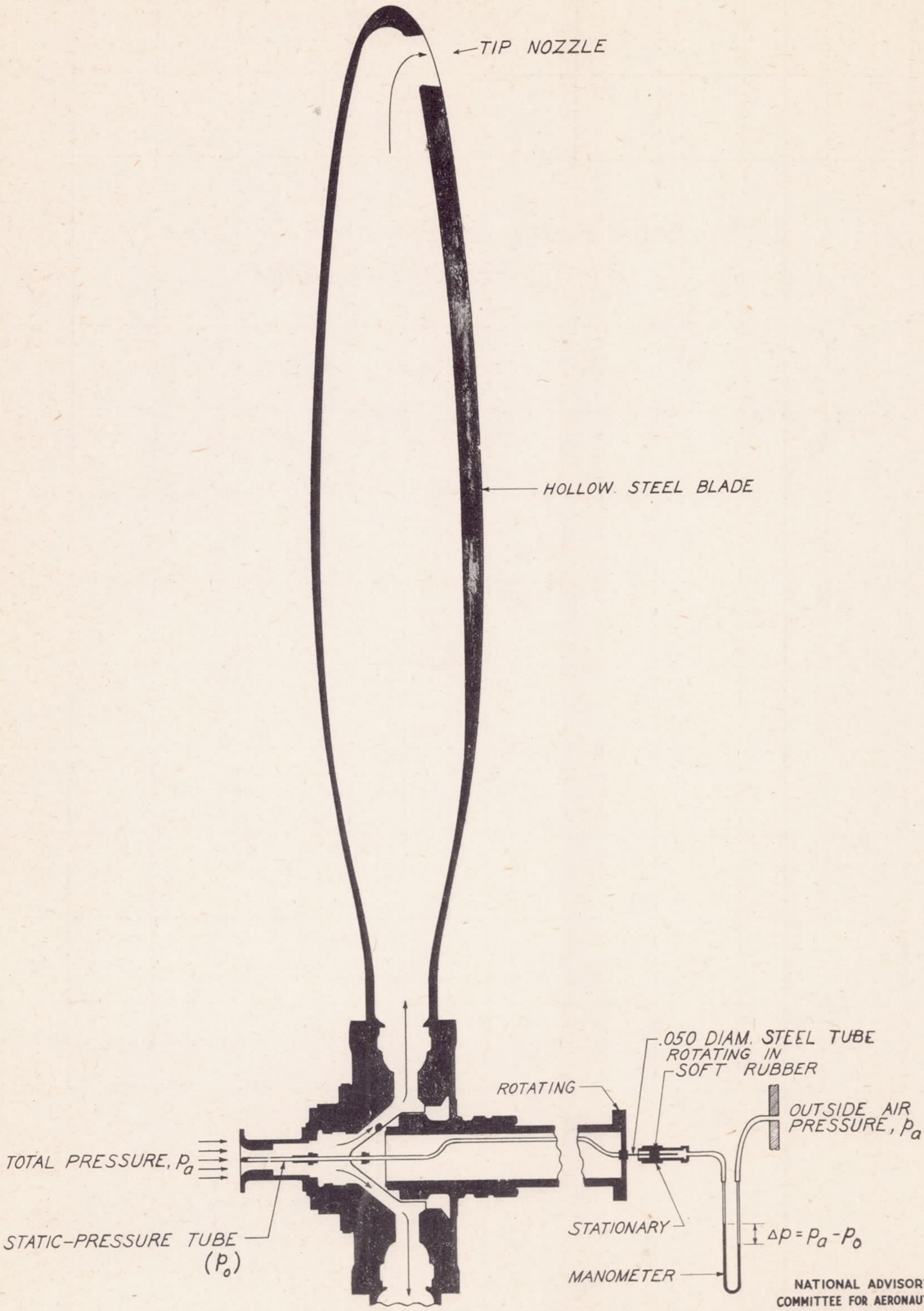

NATIONAL ADVISORY COMMITTEE FOR AERONAUTICS

FIGURE 10.— PATH OF INTERNAL FLOW THROUGH THE PROPELLER AND THE INTERNAL-MASS-FLOW METER.

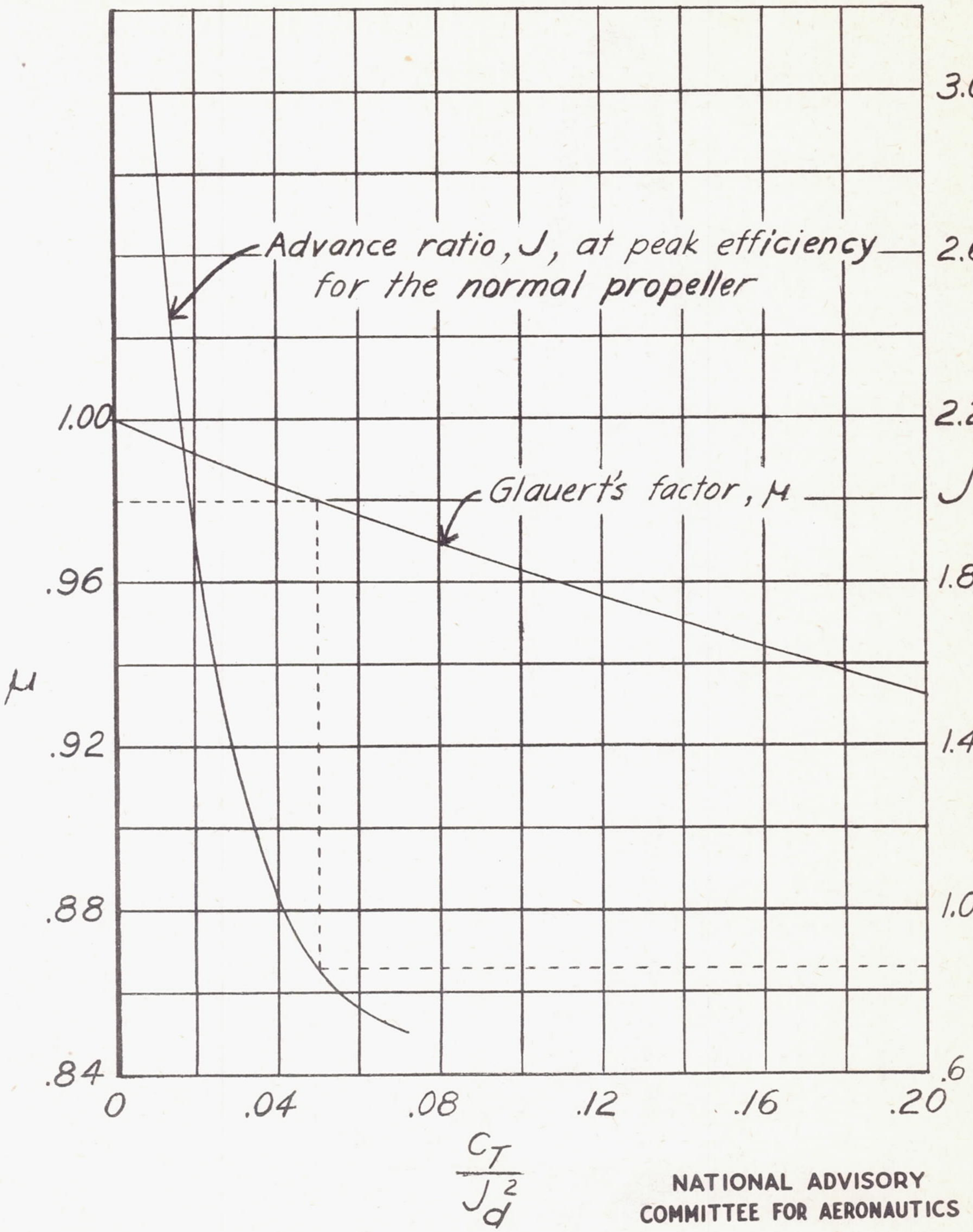

Figure 11.— Glauert's factor for correcting wind tunnel datum velocity to equivalent free airspeed for a 12.208-foot-diameter propeller in a closed 16-foot circular test jet.

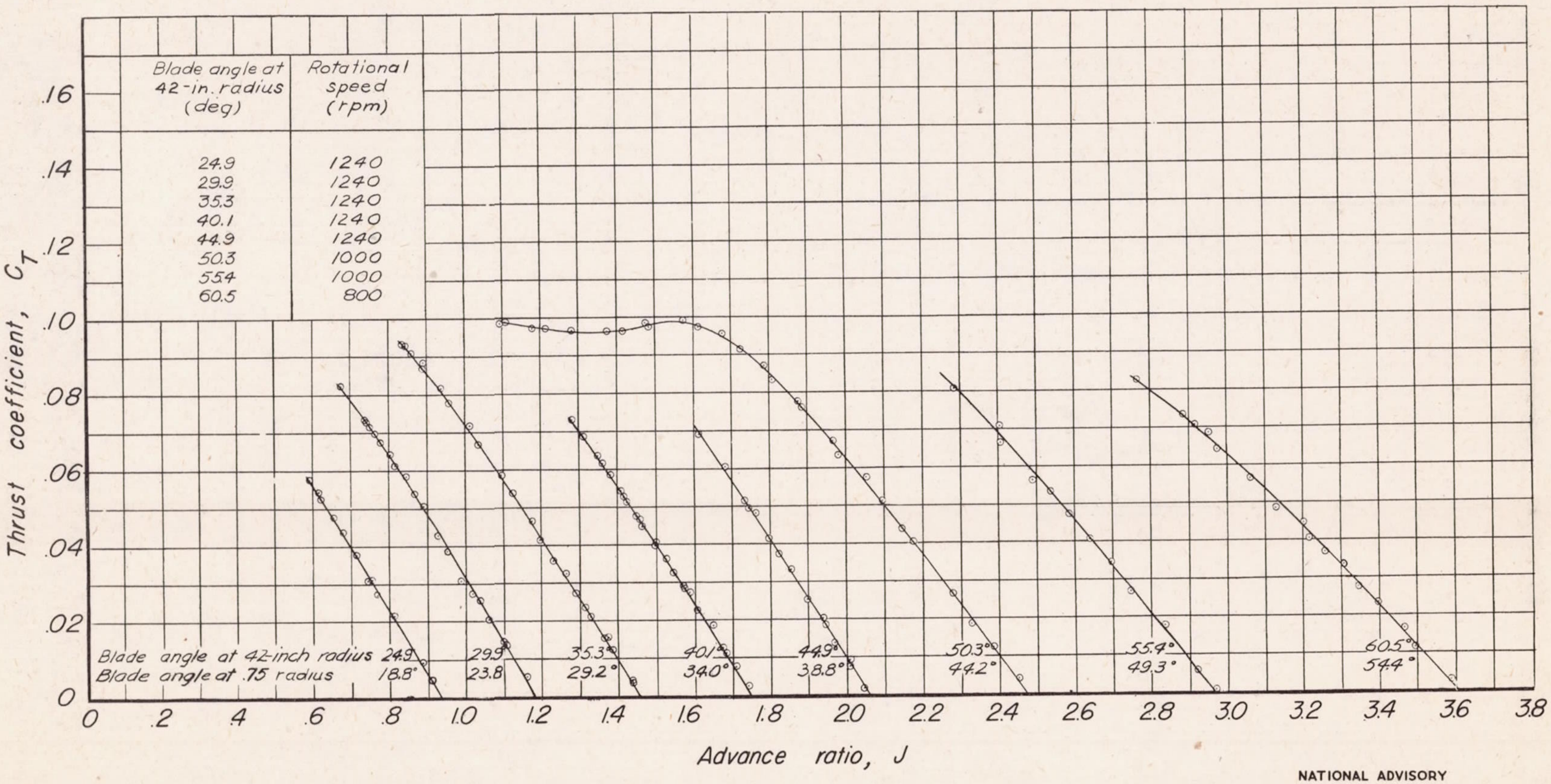

NATIONAL ADVISORY COMMITTEE FOR AERONAUTICS

Figure 12.—Variation of thrust coefficient with advance ratio. Normal propeller.

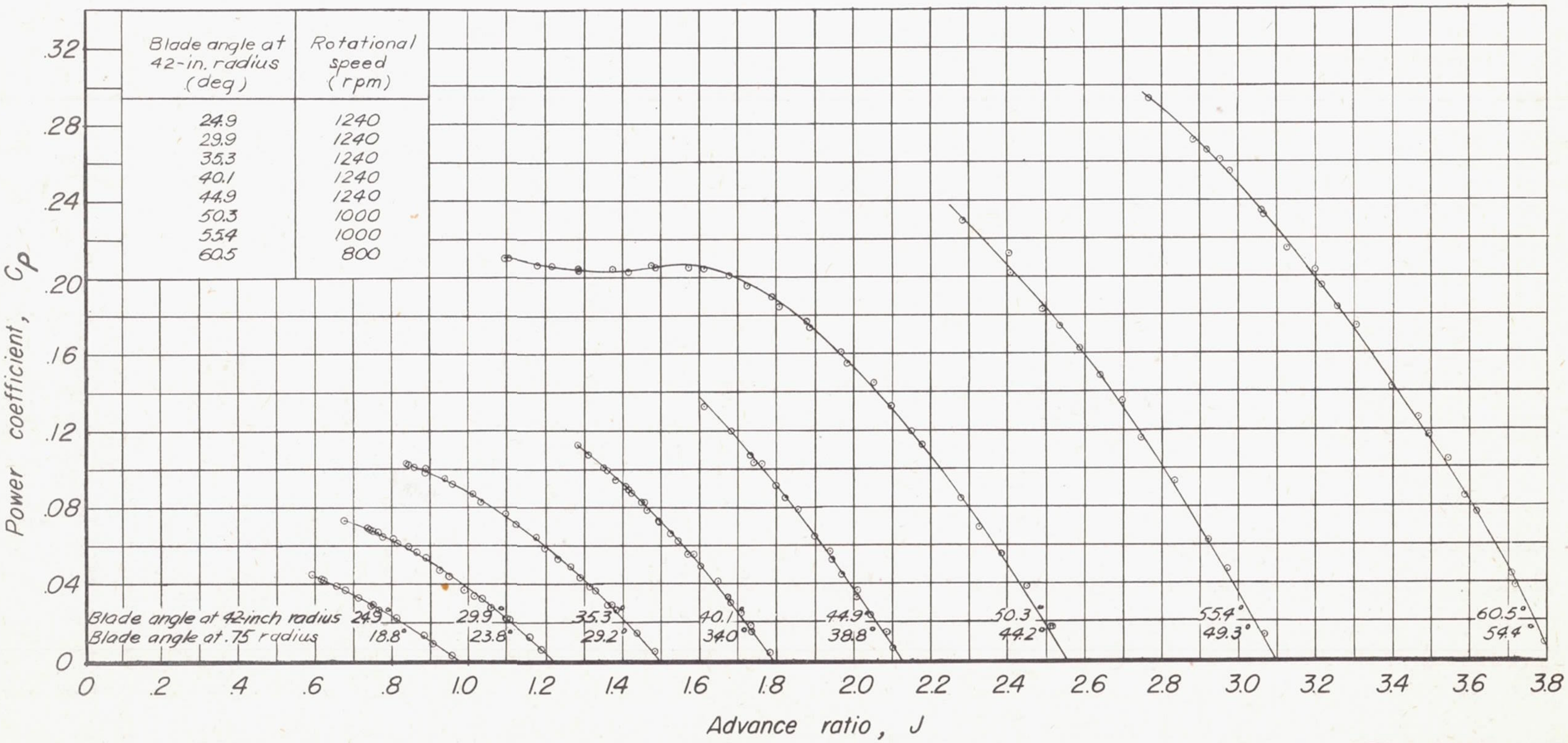

NATIONAL ADVISORY COMMITTEE FOR AERONAUTICS

Figure 13.— Variation of power coefficient with advance ratio. Normal propeller.

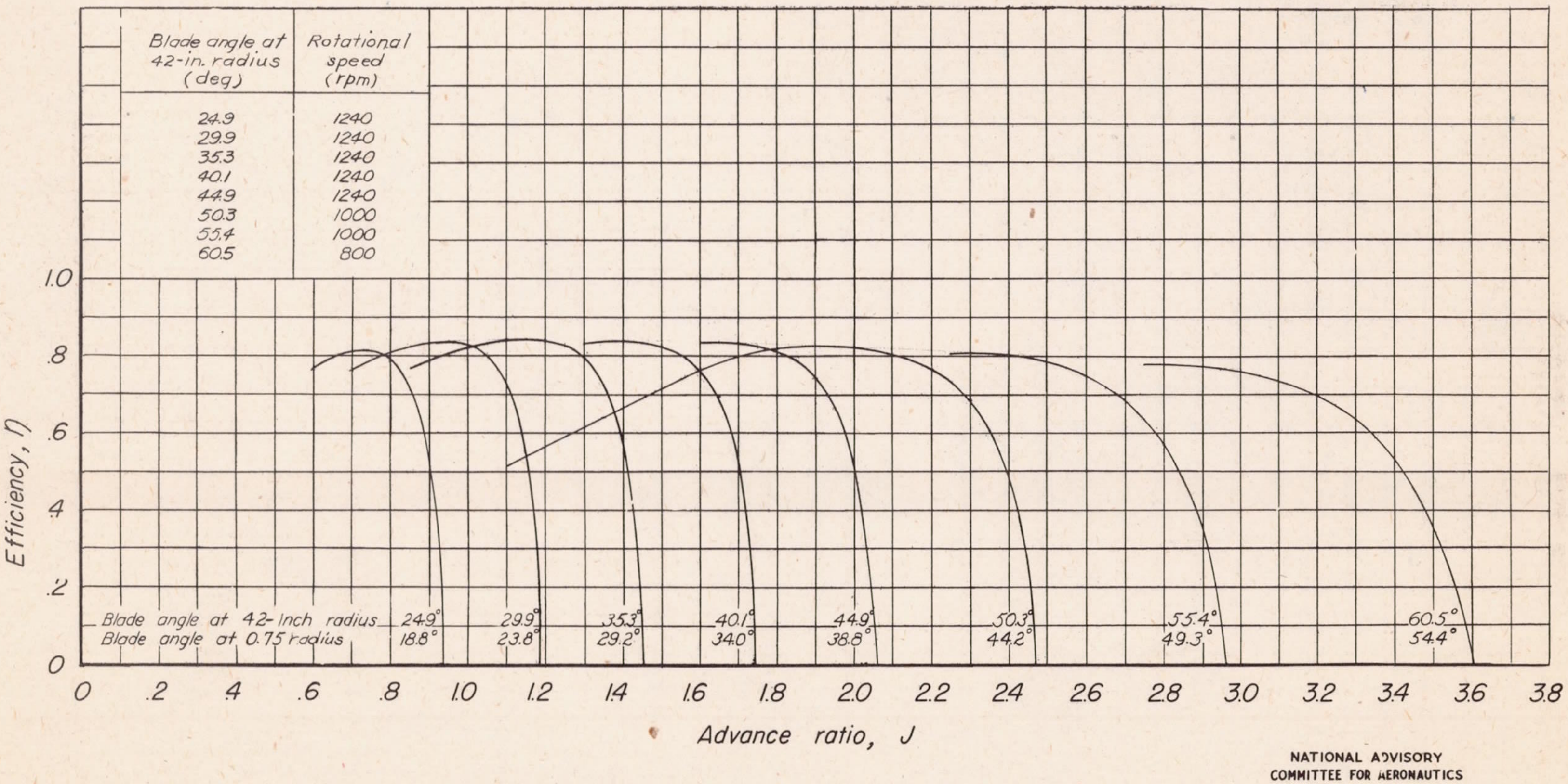

Figure 14.—Variation of propeller efficiency with advance ratio. Normal propeller.

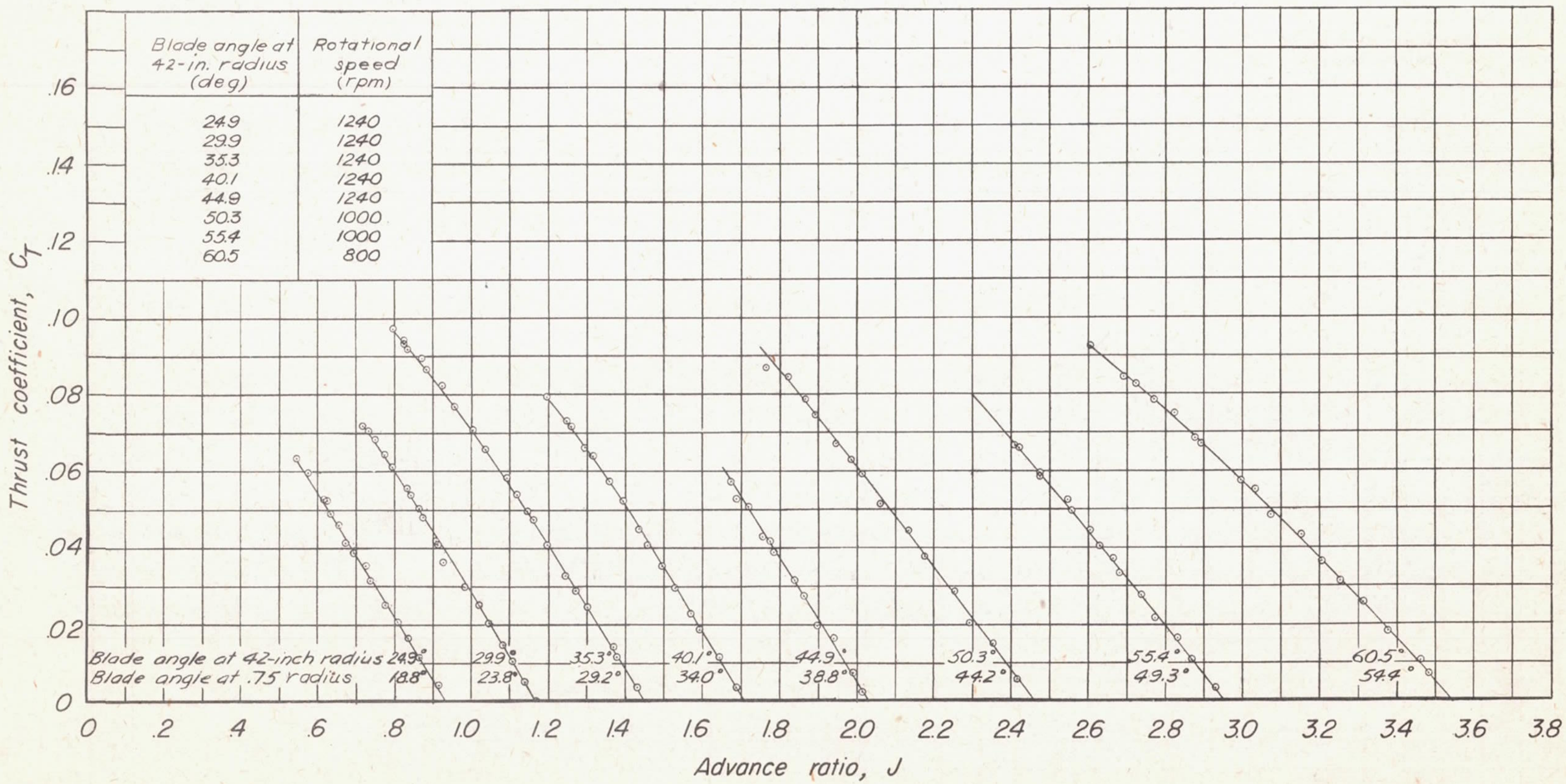

NATIONAL ADVISORY
COMMITTEE FOR AERONAUTICS

Figure 15.—Variation of thrust coefficient with advance ratio. Tips open, no de-icing flow.

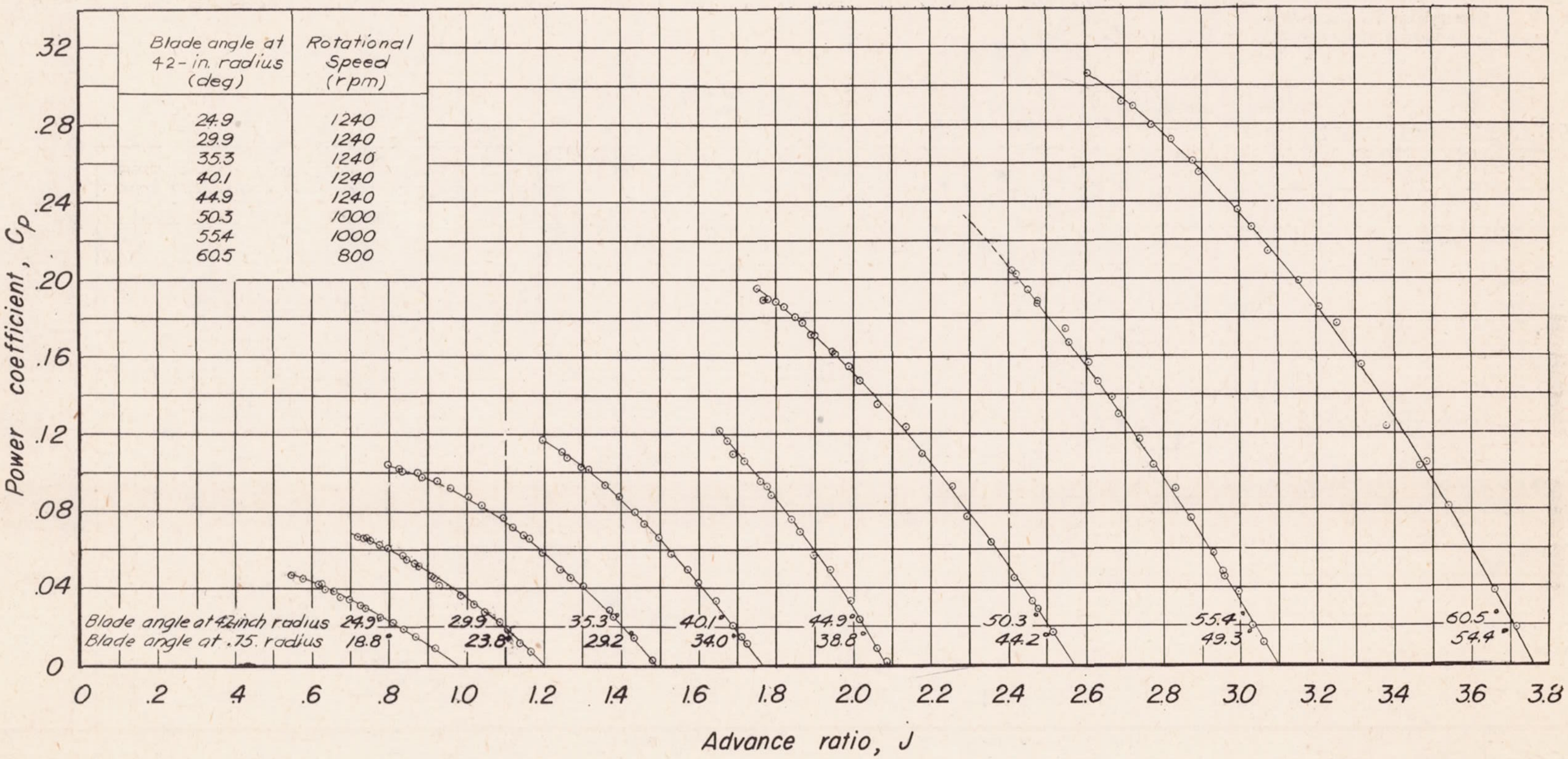

NATIONAL ADVISORY COMMITTEE FOR AERONAUTICS

Figure 16.—Variation of power coefficient with advance ratio. Tips open, no de-icing flow.

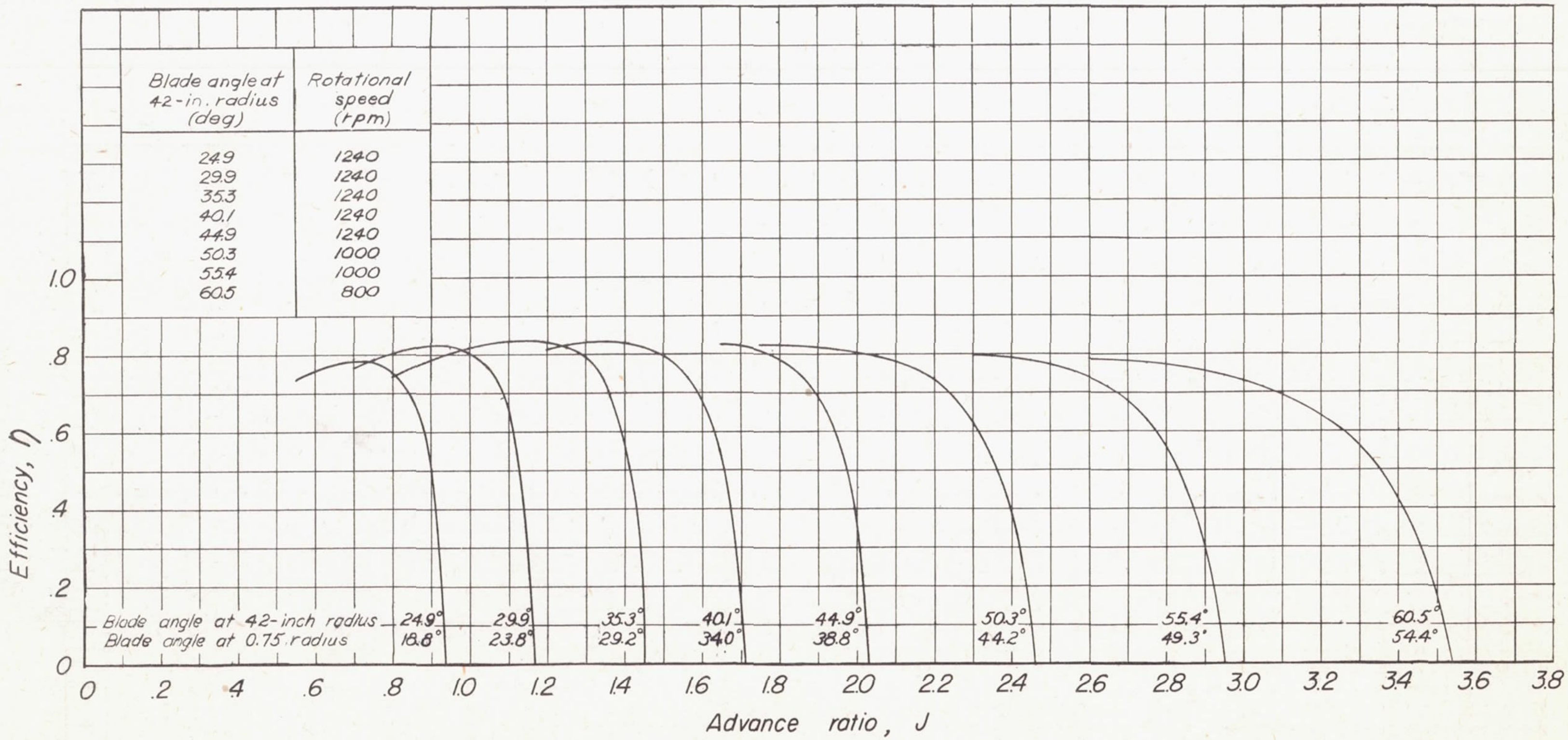

NATIONAL ADVISORY COMMITTEE FOR AERONAUTICS

Figure 17.—Variation of propeller efficiency with advance ratio. Tips open; no de-icing flow.

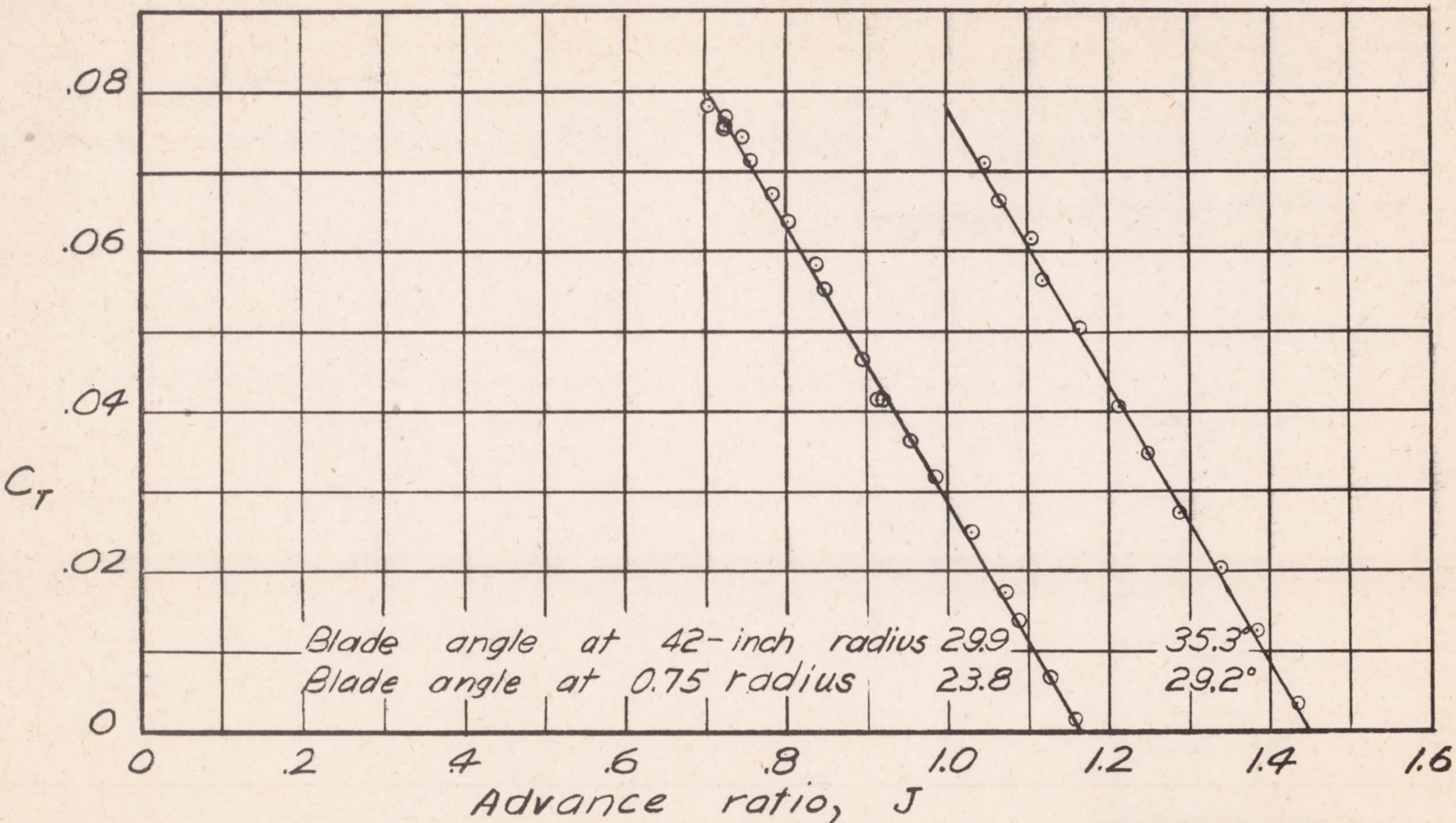

NATIONAL ADVISORY
COMMITTEE FOR AERONAUTICS

Figure 18.–Variation of thrust coefficient with advance ratio. Tips open; no de-icing flow; rotational speed, 1450 rpm.

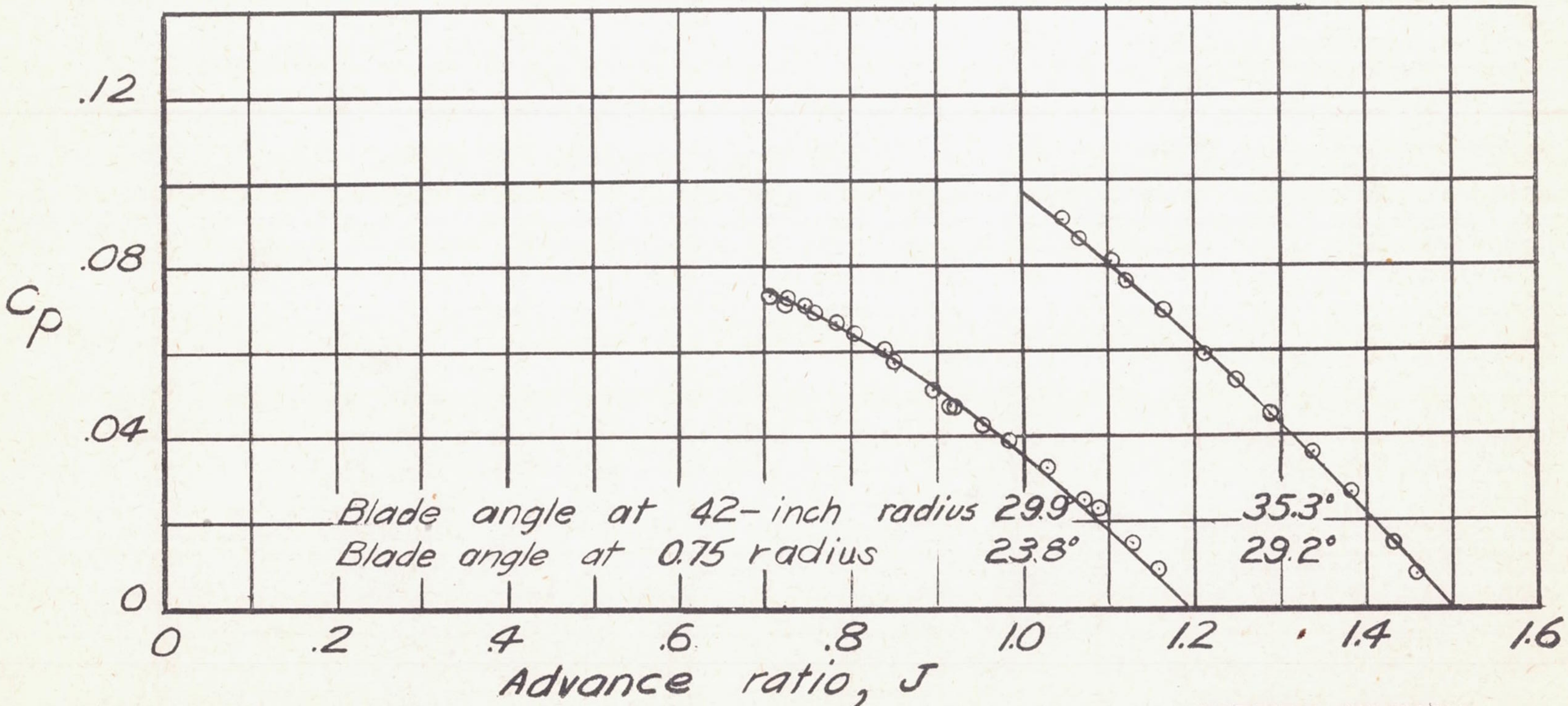

NATIONAL ADVISORY
COMMITTEE FOR AERONAUTICS

Figure 19.–Variation of power coefficient with advance ratio. Tips open; no de-icing flow; rotational speed, 1450 rpm.

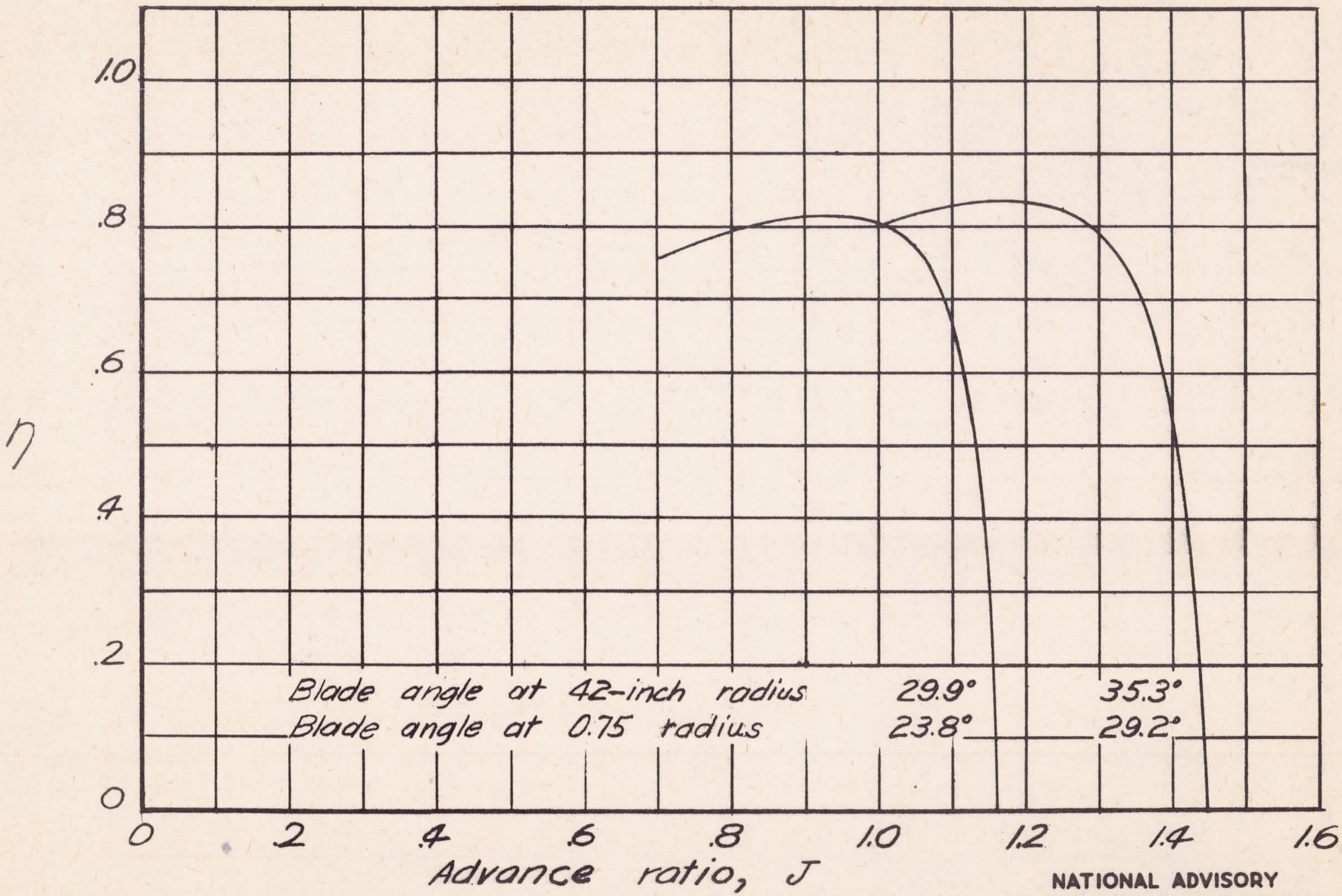

NATIONAL ADVISORY
COMMITTEE FOR AERONAUTICS

Figure 20.- Variation of propeller efficiency with advance ratio. Tips open; no de-icing flow; rotational speed, 1450 rpm.

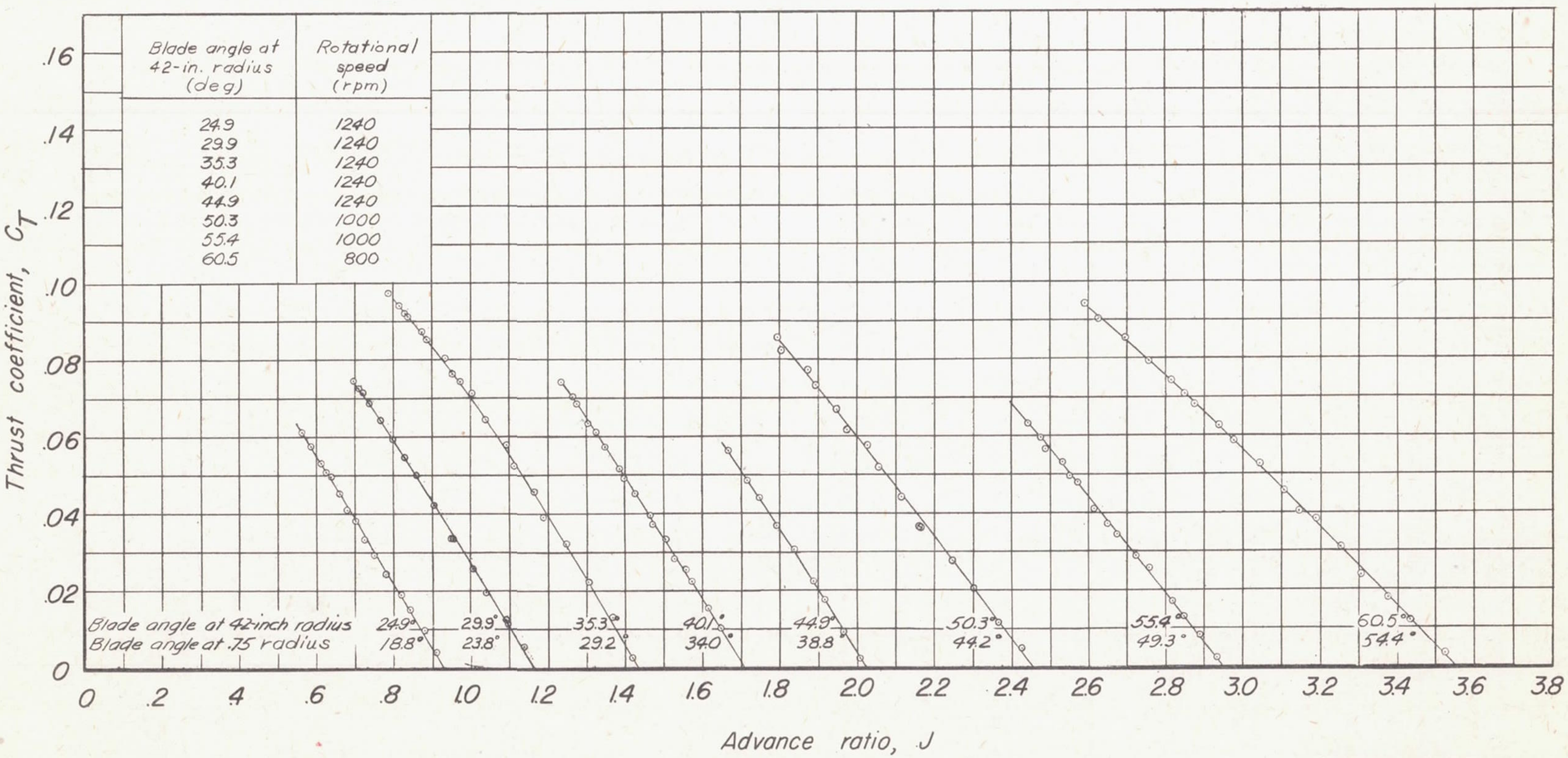

NATIONAL ADVISORY COMMITTEE FOR AERONAUTICS

Figure 21.—Variation of thrust coefficient with advance ratio. Propeller with de-icing air flow

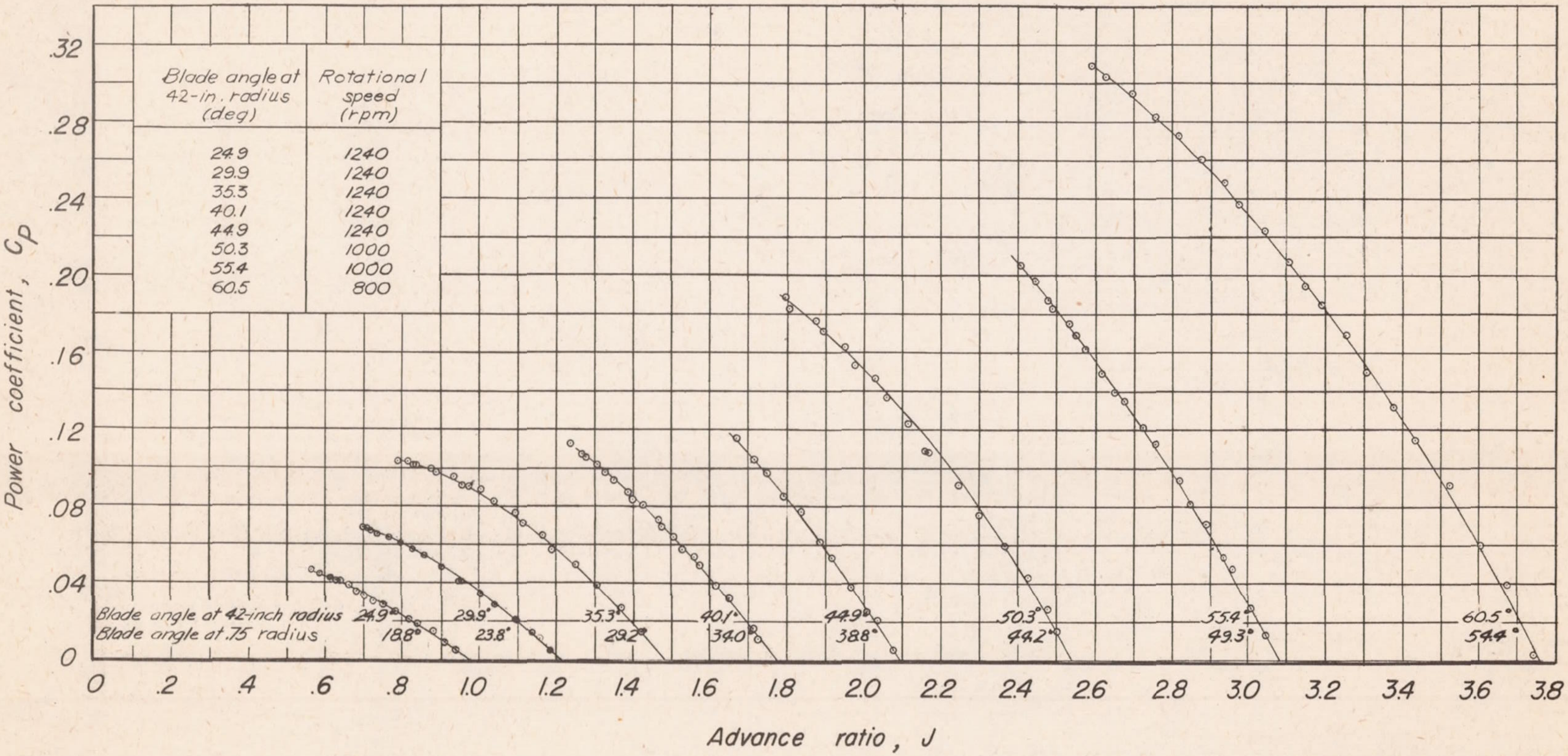

NATIONAL ADVISORY COMMITTEE FOR AERONAUTICS

Figure 22.— Variation of power coefficient with advance ratio. Propeller with de-icing air flow.

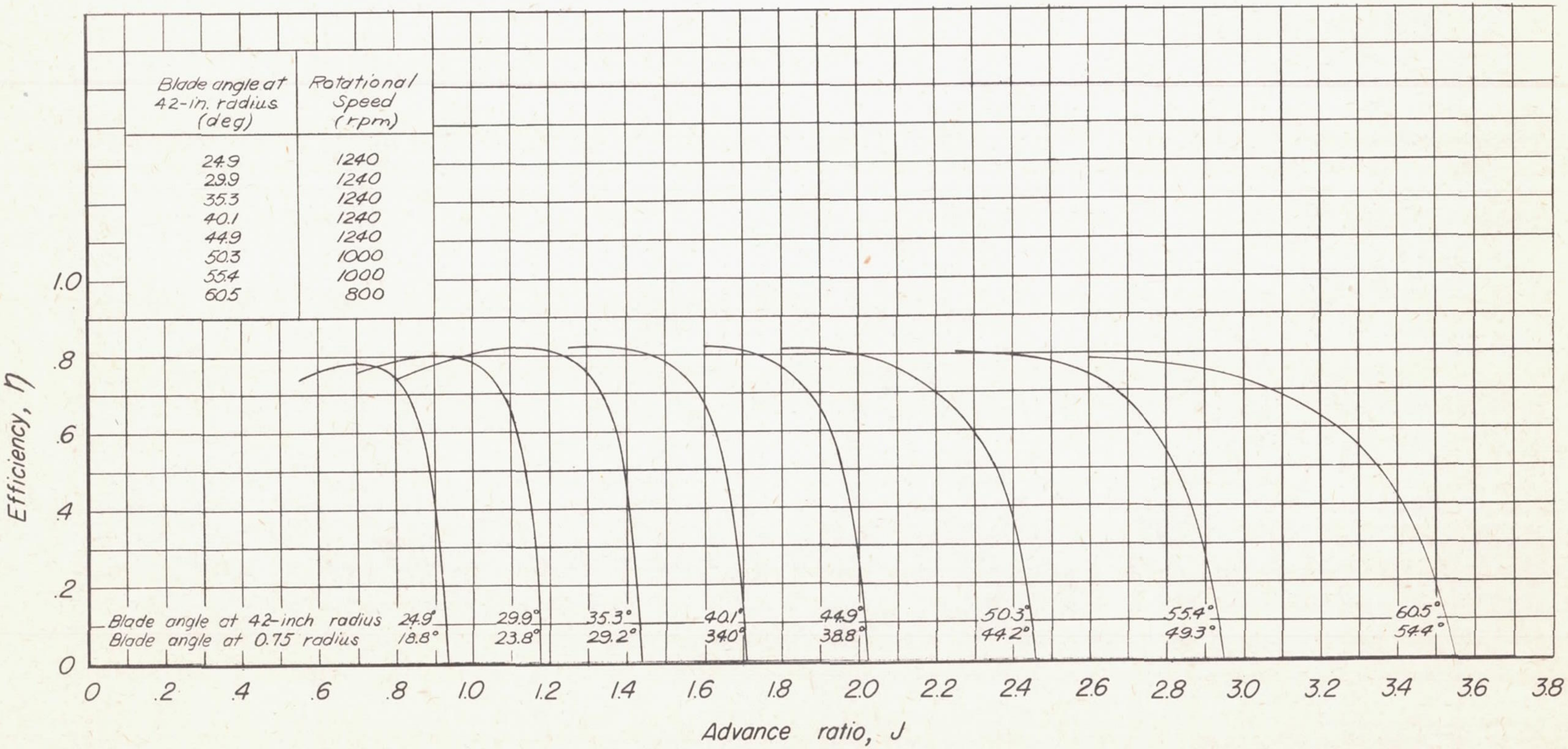

NATIONAL ADVISORY COMMITTEE FOR AERONAUTICS

Figure 23.—Variation of propeller efficiency with advance ratio. Propeller with de-icing air flow.

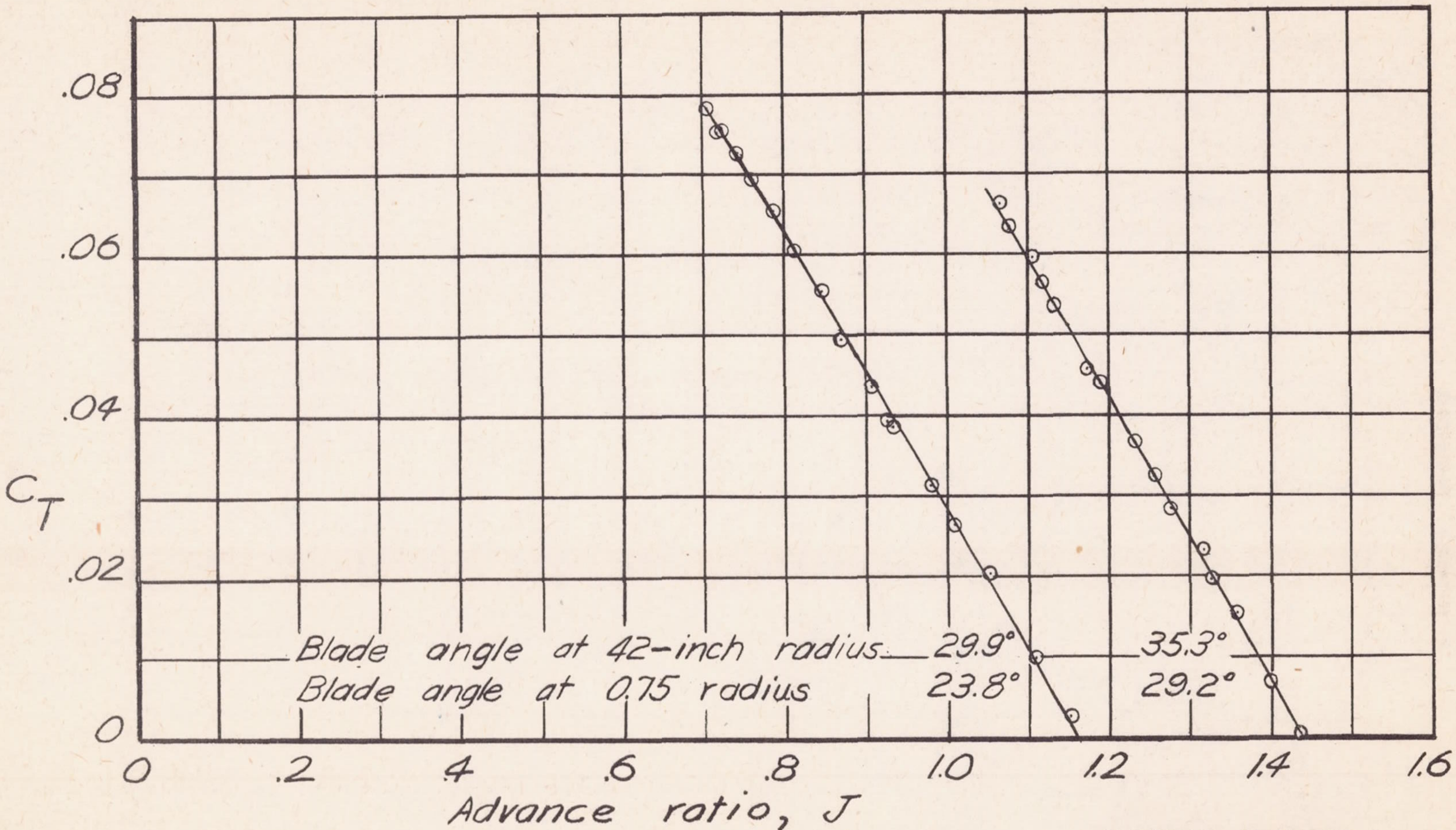

NATIONAL ADVISORY
COMMITTEE FOR AERONAUTICS

Figure 24.- Variation of thrust coefficient with advance ratio. Propeller with de-icing air flow; rotational speed, 1450 rpm.

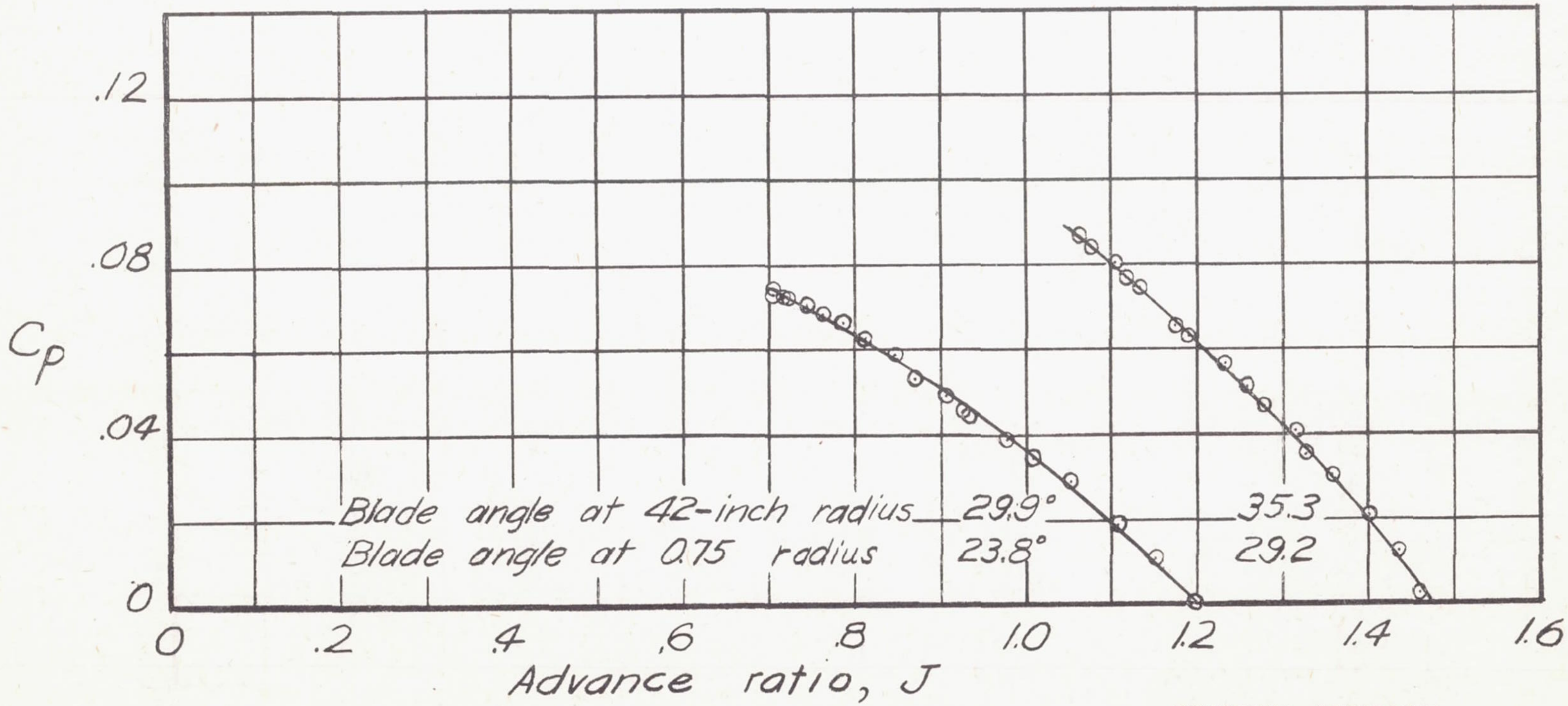

NATIONAL ADVISORY
COMMITTEE FOR AERONAUTICS

Figure 25.- Variation of the power coefficient with advance ratio. Propeller with de-icing air flow; rotational speed, 1450 rpm.

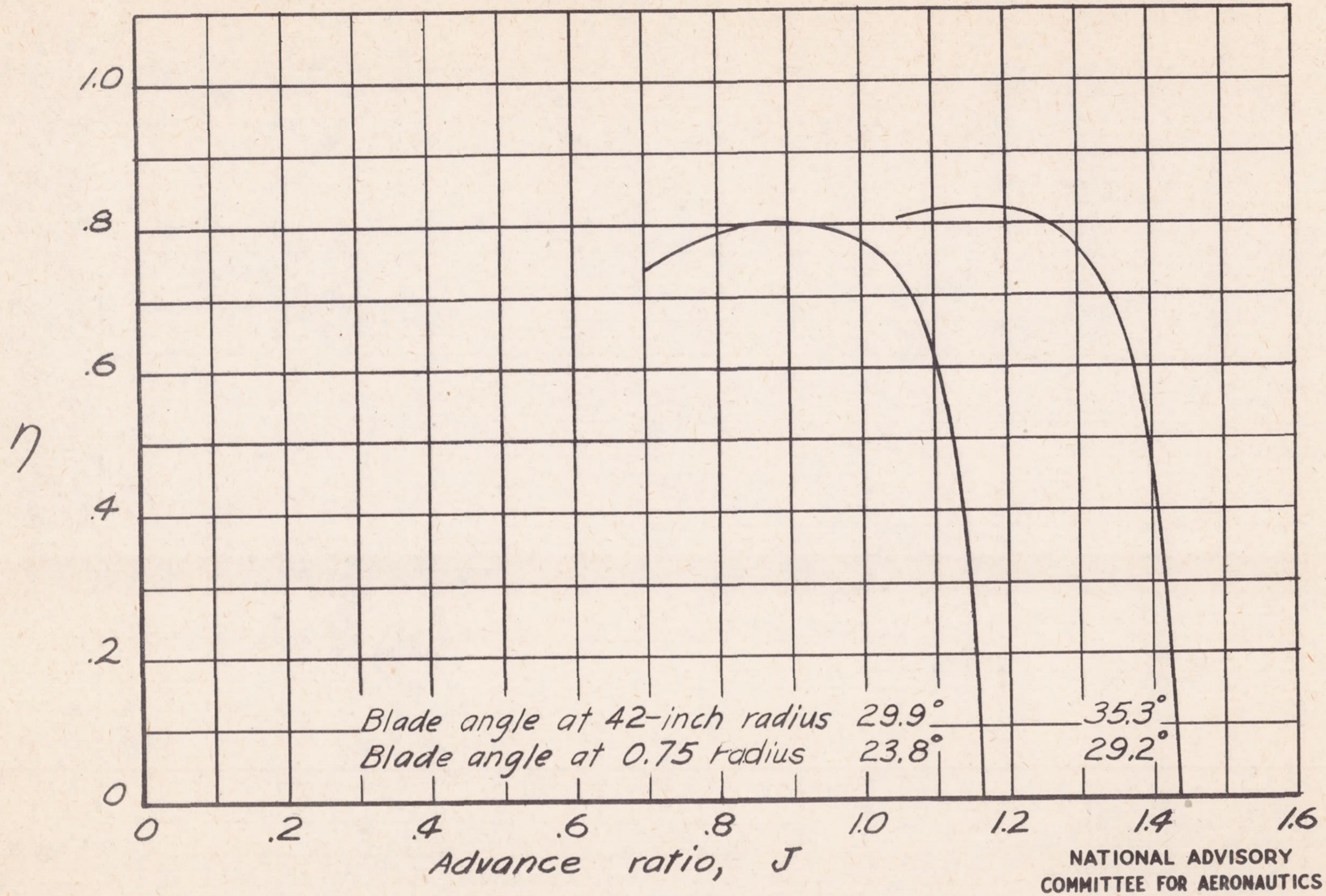

NATIONAL ADVISORY COMMITTEE FOR AERONAUTICS

Figure 26.- Variation of propeller efficiency with advance ratio. Propeller with de-icing air flow; rotational speed, 1450 rpm.

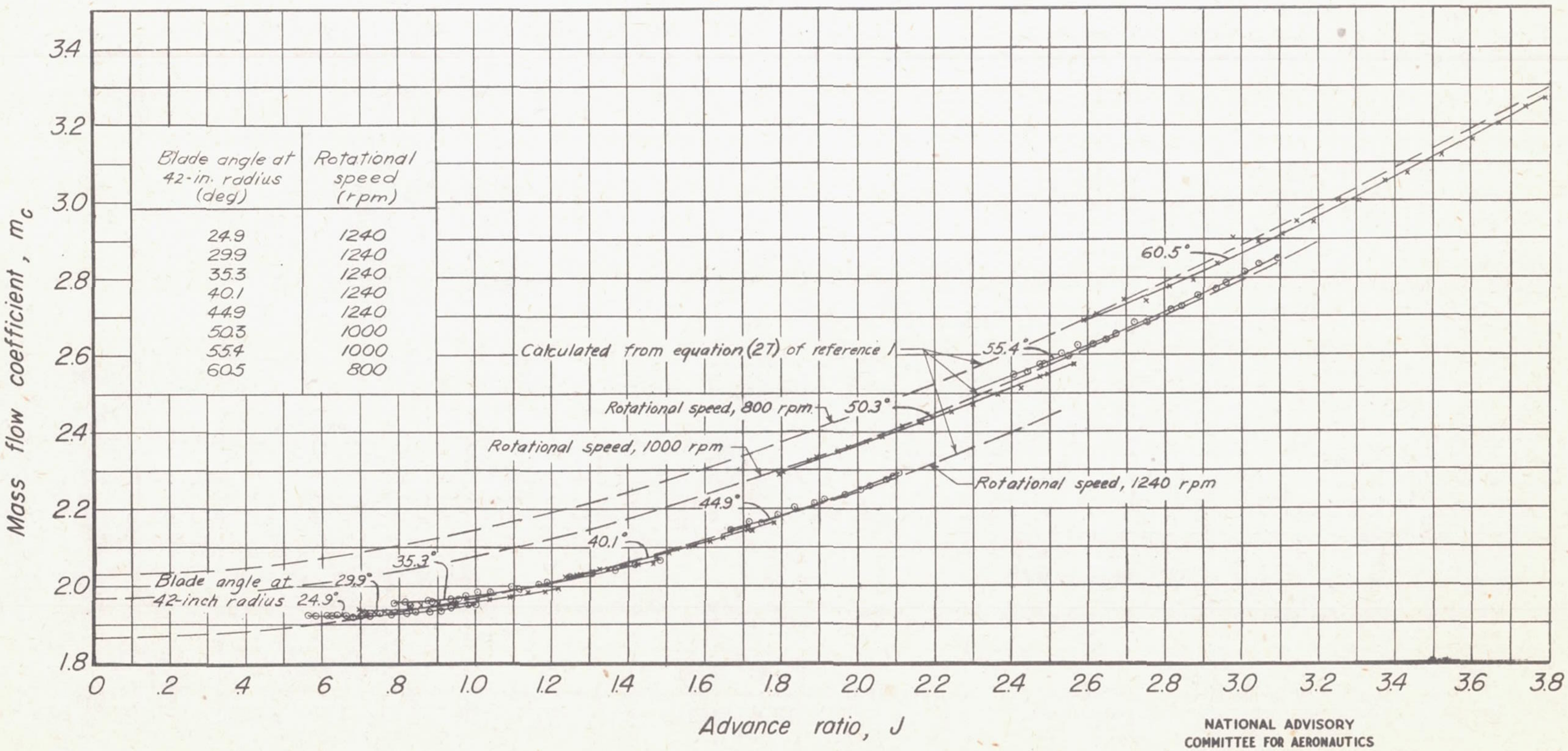

Figure 27.—Variation of the coefficient of mass flow of de-icing air with advance ratio.

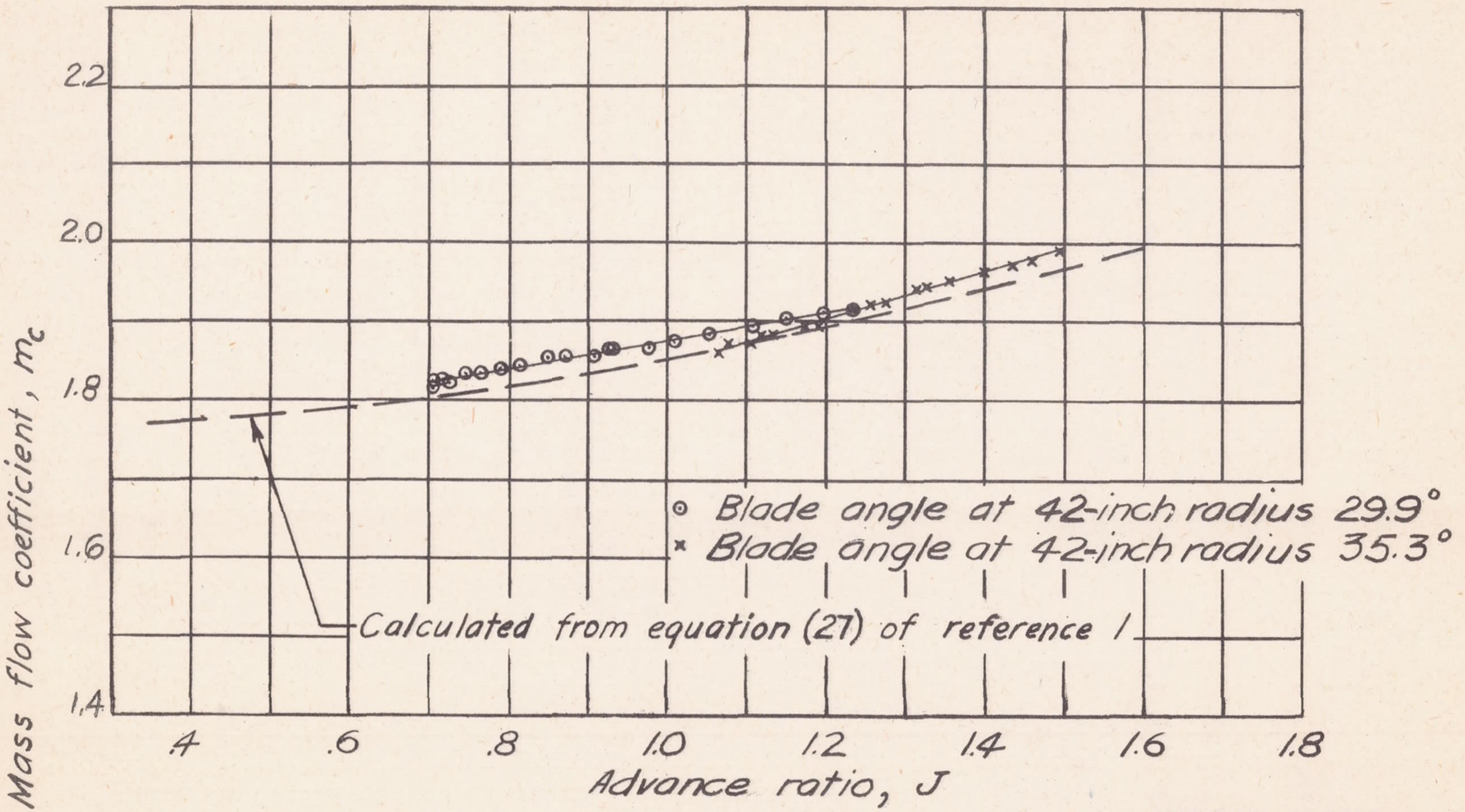

NATIONAL ADVISORY
COMMITTEE FOR AERONAUTICS

Figure 28.— Variation of the coefficient of mass flow of de-icing air with advance ratio. Rotational speed, 1450 rpm.

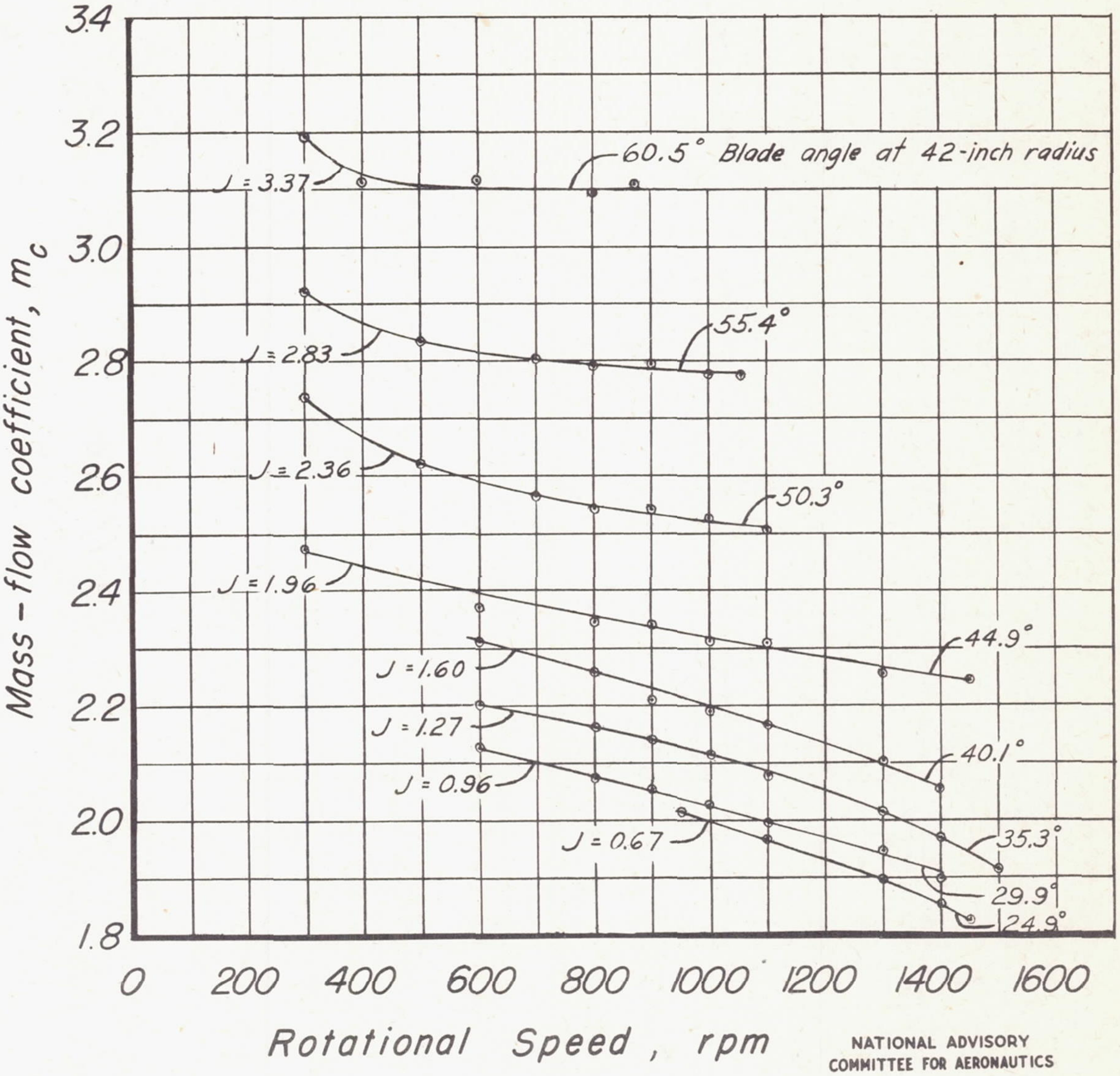

Figure 29.—Variation of the coefficient of mass flow of de-icing air with rotational speed.

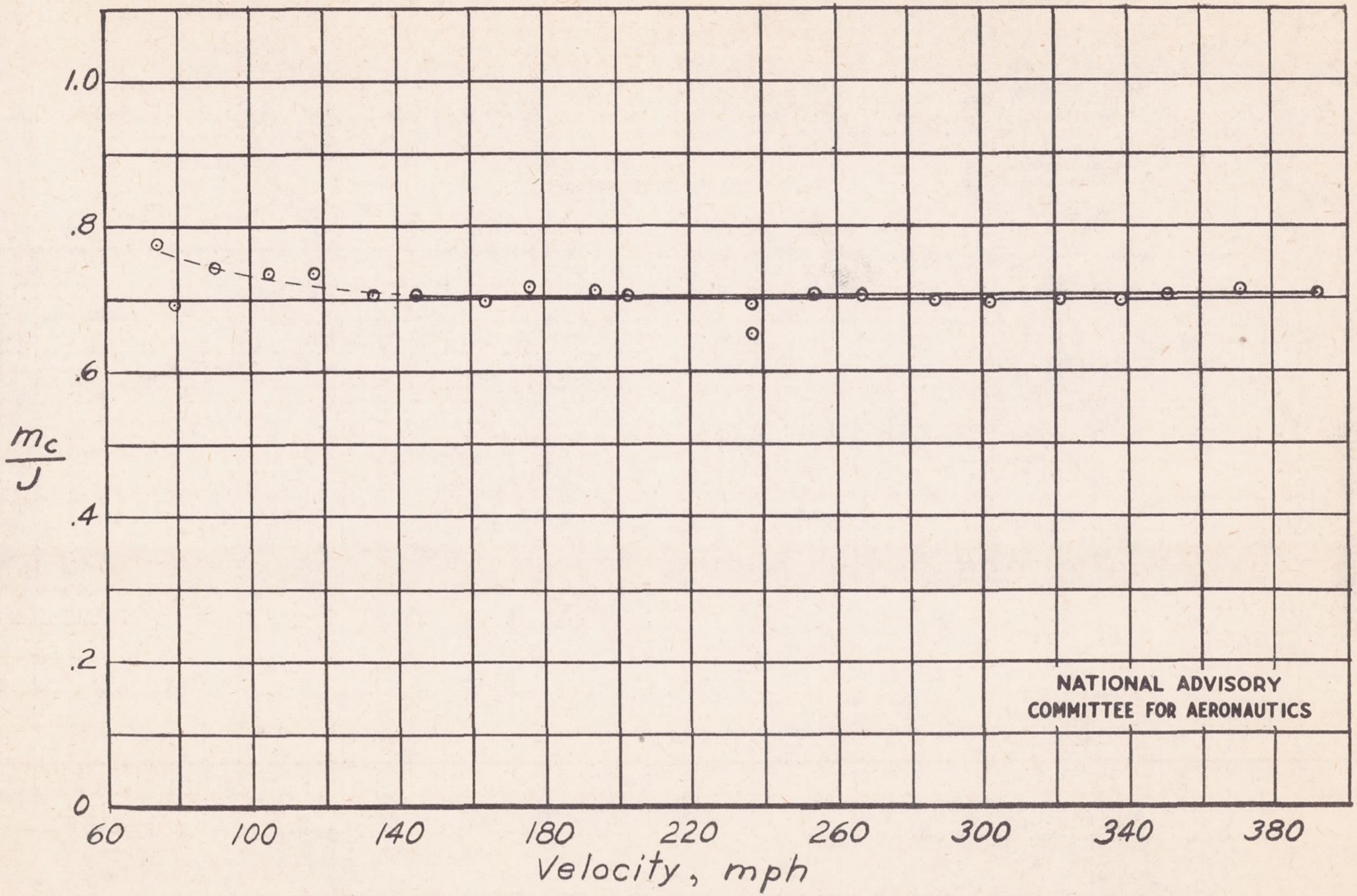

Figure 30.- Coefficient of mass flow of de-icing air for infinite advance ratio (rotational speed very low).

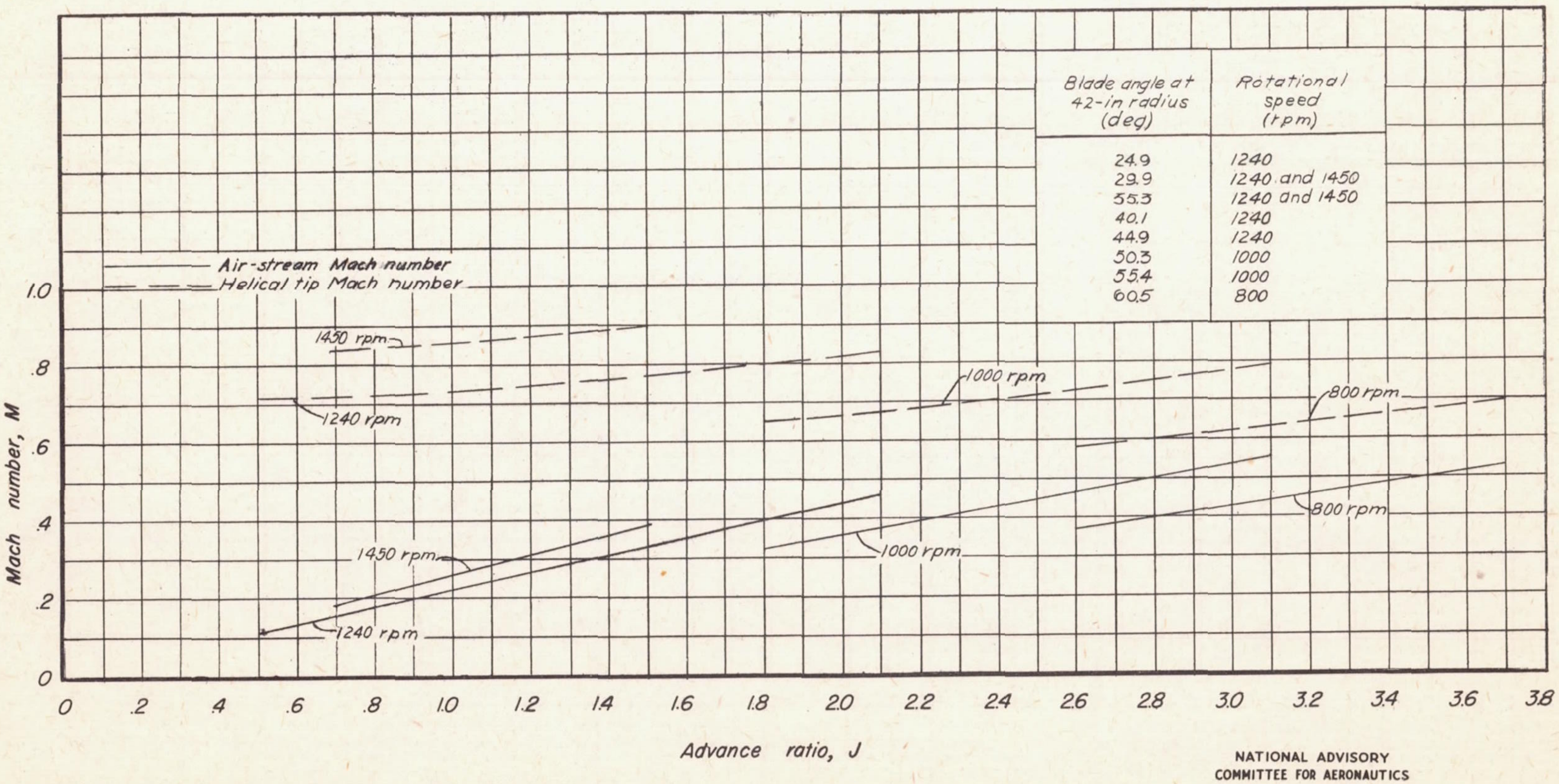

Figure 31.— Variation of air-stream Mach number and helical tip Mach number with advance ratio.

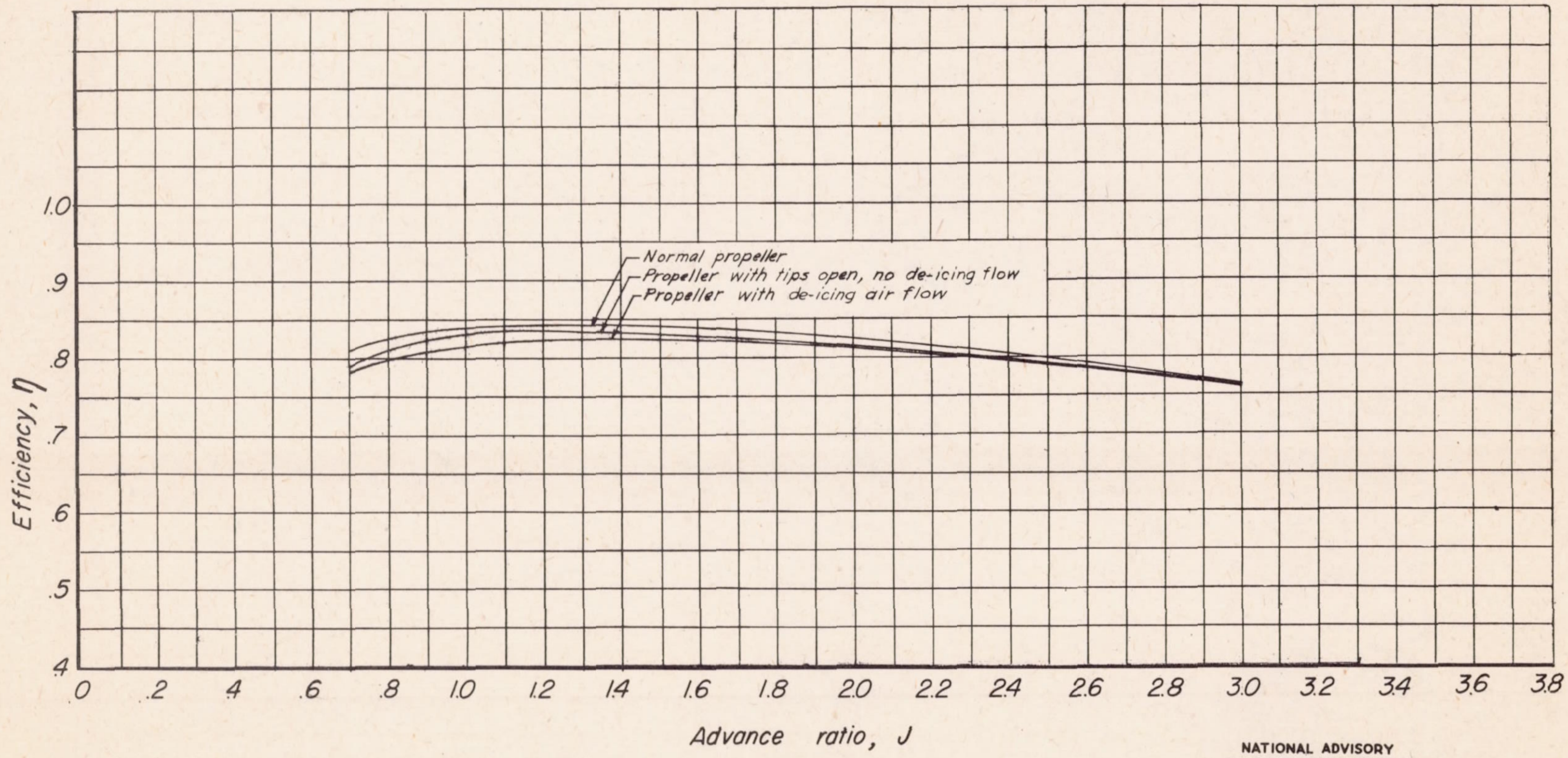

NATIONAL ADVISORY COMMITTEE FOR AERONAUTICS

Figure 32.— A comparison of the envelope curves of propeller efficiency.